catalysts

MDPI

Review

# The Role of Surface Texture on the Photocatalytic $H_2$ Production on $TiO_2$

**Francesco Pellegrino *,†, Fabrizio Sordello †, Marco Minella †, Claudio Minero and Valter Maurino**

Department of Chemistry and NIS—Nanostructured Interfaces and Surfaces Interdepartmental Centre, University of Turin, via Pietro Giuria 7, 10125 Turin, Italy; fabrizio.sordello@unito.it (F.S.); marco.minella@unito.it (M.M.); claudio.minero@unito.it (C.M.); valter.maurino@unito.it (V.M.)

* Correspondence: francesco.pellegrino@unito.it; Tel.: +39-011-6705218

† These authors contributed equally to the work.

Received: 31 October 2018; Accepted: 25 December 2018; Published: 2 January 2019


**Abstract:** It has been often reported that an efficient and green photocatalytic dissociation of water under irradiated semiconductors likely represents the most important goal for modern chemistry. Despite decades of intensive work on this topic, the efficiency of the water photolytic process under irradiated semiconductors is far from reaching significant photocatalytic efficiency. The use of a sacrificial agent as hole scavenger dramatically increases the hydrogen production rate and might represent the classic "kill two birds with one stone": on the one hand, the production of hydrogen, then usable as energy carrier, on the other, the treatment of water for the abatement of pollutants used as sacrificial agents. Among metal oxides, $TiO_2$ has a central role due to its versatility and inexpensiveness that allows an extended applicability in several scientific and technological fields. In this review we focus on the hydrogen production on irradiated $TiO_2$ and its fundamental and environmental implications.

**Keywords:** hydrogen; photocatalytic reforming; $TiO_2$; water photosplitting; surface

## 1. Introduction

From the perspective of our ancestors (and of the billions of underprivileged people living in the developed and developing world), we are living an unprecedented golden age thanks to the large availability of fossil fuels that provide economical energy sources. This is translated into a large pool of available goods and services, which are becoming more and more available to an increasing share of the world population. The lifestyle of wealthy nations is simultaneously very appealing and dependent on energy. This pushes an increasing fraction of the population to adopt it, and to cope with its direct and indirect drawbacks, namely stress, obesity, pollution and finally, global warming.

In the 1970s, the Kippur and the Iran–Iraq wars created a sense of awareness about the dependence on fossil fuels and the consequences of their eventual depletion, and pushed the research to find alternatives. Almost 50 years later, 85% of the world's primary energy is still coming from fossil fuels [1], but we are presently facing a subtler threat related to global warming. To have at least a 50% chance of keeping warming below 2 °C throughout this century, two-thirds of the global fossil fuels reserves must remain untouched [2,3]. These "forbidden" reserves represent the so-called "unburnable carbon". This should further push researchers, but also policy makers, to find sustainable alternatives, because the transition should be completed significantly before the depletion of fossil fuels reserves.

Then again this poses another problem to citizens and policy makers when comparing different technologies. Usually such comparisons are based on performance and costs. Liquid fossil fuels are relatively cheap and have an unparalleled energy density, compared with hydrogen and batteries [4].

However, on the price figure the costs of the effects of pollution and global warming should be also taken into account, even if their accurate determination is cumbersome.

In this respect, hydrogen would be a suitable alternative energy carrier, and its employment was suggested by Jules Verne in his 1874 novel, *L'île mystérieuse*. In this novel, a main character says: "I believe that water will one day be employed as fuel, that hydrogen and oxygen which constitute it, used singly or together, will furnish an inexhaustible source of heat and light, of an intensity of which coal is not capable. [...] Water will be the coal of the future".

Nonetheless, hydrogen on the Earth's crust only exists in the form of compounds, and cannot be mined or extracted directly, but must be produced employing energy from other vectors or from energy sources. If hydrogen were obtained from renewable intermittent sources, then it would represent a useful energy carrier to mitigate peak production and stabilize the energy network. Nevertheless, as outlined by Armaroli and Balzani in one of their excellent reviews [5], it is highly unlikely that hydrogen as an energy vector will be sufficient to maintain the current mobility standards in wealthy countries. More probably hydrogen will be one of the many solutions needed to complete the energy transition from fossil fuels. Its relative importance compared with other technologies will depend globally on the scientific and technologic advances that we will experience in the next decades, and regionally also on the peculiarity of the area considered, such as energy demand, availability and intermittency of other sources, such as hydro, wind, solar and biomasses. Even though a future global era of hydrogen seems improbable now, in certain local communities it could play a relevant role (vide infra).

Even though the future of hydrogen as widespread energy vector remains unclear, from a more fundamental point of view, the understanding of the water photosplitting and photoreforming processes could have many positive repercussions in other fields, such as photovoltaics, batteries and fuel cells. In the present review we will concentrate our attention on the hydrogen production on $TiO_2$, its fundamental and environmental implications and on emerging new strategies to improve its production.

### *1.1. Semantics and Thermodynamics*

Many different processes can be listed under the banner of hydrogen photoproduction. First, considerations about the reaction products suggest a subdivision into two main groups: (*i)* hydrogen production via water photosplitting, where $O_2$ is the product of the anodic semireaction; (*ii)* hydrogen production via photoreforming, where $CO_2$ instead of $O_2$ is yielded. The reaction involved in (*i)*, for liquid and vapor water, is associated to a positive Gibbs free energy variation [6]:

$$2\ H_2O_{(l)} \rightarrow 2\ H_{2(g)} + O_{2(g)} \qquad \Delta G^0 = 237\ \text{kJ mol}^{-1} \tag{1}$$

$$2\ H_2O_{(g)} \rightarrow 2\ H_{2(g)} + O_{2(g)} \qquad \Delta G^0 = 229\ \text{kJ mol}^{-1} \tag{2}$$

This means that the reaction is not spontaneous at room temperature, but requires a significant energy input, which can be chemical, electrochemical or electromagnetic (Figure 1). To perform water photosplitting, the energy required will be provided in the form electromagnetic energy, i.e., light. Considering that two electrons are required to oxidize one water molecule to $O_2$, the energy required is to be delivered by two photons, then the minimum photon energy will be 1.23 eV, i.e., ≈1010 nm:

$$photon\ energy\ (eV) = \frac{\Delta G^0}{2N_A e}$$

where $N_A$ is the Avogadro constant and $e$ is the electron's elementary charge. But, because $O_2$ is the product of water oxidation, the whole process is actually a *four*-photon, *four*-electron process. Consequently, to promote water cleavage in an electrolyzer, the energy constraint will be overcome

thanks to an external bias, which must be larger than 1.23 V, because of the standard potentials of the couples:

$$2\,H^{+}_{(aq)} + 2\,e^{-} \rightarrow H_{2(g)} \qquad E^{0} = 0.000\ V \tag{3}$$

$$4\,H^{+}_{(aq)} + O_{2(g)} + 4\,e^{-} \rightarrow 2\,H_2O_{(g)} \qquad E^{0} = 1.229\ V \tag{4}$$

Considering that

$$\Delta G^{0} = nFE^{0} \tag{5}$$

with n = 2 in the case of water, Equation (5) further demonstrates how the thermodynamic requirements of Equations (1)–(4) are linked together [7]. Due to its positive Gibbs energy variation, water photosplitting is a photosynthetic reaction. For this reason, it could be legitimately considered a form of artificial photosynthesis, and, in fact, the anodic semireaction involves the oxidation of water and the formation of molecular oxygen, while on the cathodic side there is the formation of a fuel, $H_2$, finalizing the transformation of electromagnetic energy into chemical energy.

In the case of hydrogen production from photoreforming, a hydrogen-containing organic compound—such as methanol—produces hydrogen and carbon dioxide:

$$CH_3OH_{(l)} + H_2O_{(l)} \rightarrow 3\,H_{2(g)} + CO_{2(g)} \qquad \Delta G^{0} = 8\ kJ\ mol^{-1} \tag{6}$$

In this latter case the Gibbs free energy variation is still positive, but its value is almost two orders of magnitude less than in the case of Equation (1). The reason is the great stability of carbon dioxide, which has Gibbs' free energy of formation, $\Delta G^{0}_{f}$, of $-394$ kJ mol$^{-1}$ [8]. On the other hand, water also has a quite large $\Delta G^{0}_{f}$ (water formation reaction is the reverse of Equation (1)). Therefore, depending on the particular organic compound, its reforming could be either endergonic or exergonic, according to the number of water and carbon dioxide molecules involved in the reaction. For example, formic acid and glycerol are characterized by a $H_2O$ to $CO_2$ ratio of 0 and 1, respectively, and in both cases their reforming is a downhill reaction:

$$HCOOH \rightarrow H_2 + CO_2 \qquad \Delta G^{0} = -83\ kJ\ mol^{-1} \tag{7}$$

$$C_3H_8O_3 + 3\,H_2O \rightarrow 7\,H_2 + 3\,CO_2 \qquad \Delta G^{0} = -300\ kJ\ mol^{-1} \tag{8}$$

whereas in the case of ethanol and propan-2-ol, where the $H_2O$ to $CO_2$ ratio is larger than 1, the Gibbs free energy of their reforming is positive:

$$C_3H_8O + 5\,H_2O \rightarrow 9\,H_2 + 3\,CO_2 \qquad \Delta G^{0} = 183\ kJ\ mol^{-1} \tag{9}$$

$$C_2H_6O + 3\,H_2O \rightarrow 6\,H_2 + 2\,CO_2 \qquad \Delta G^{0} = 97\ kJ\ mol^{-1} \tag{10}$$

Therefore, when the previous reforming reaction are promoted by light we can be in the presence of either photosynthetic or photocatalytic processes, depending on the $\Delta G$. Nevertheless, we feel that the claim of artificial photosynthesis in the cases of reactions (6), (9) and (10) would be exaggerated, even though their positive $\Delta G$ would make such a claim technically correct. In the case of organic reforming the oxidation potentials are less positive, and the kinetics of reaction less complicated compared with water oxidation, even though also in these cases multielectron and multiproton transfers are involved (Figure 1).

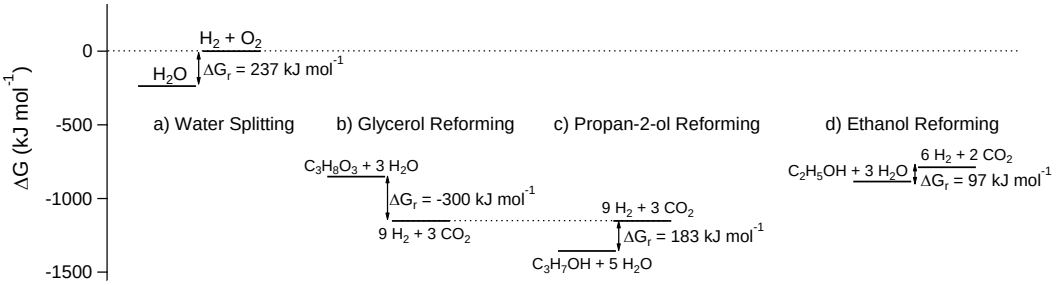


**Figure 1.** Energy diagram for water splitting and for the reforming of selected organic compounds.

Accordingly, also the minimum photon energy required will be lower. Focusing our attention to $TiO_2$, its band gap is larger than 3 eV; therefore, its excitation requires UV photons, or in terms of energy 300 kJ $mol^{-1}$, which is larger than the $\Delta G^0$ of all the reactions considered until now (Figure 2a). Considering that reactions 1–10 involve all multiple electron transfers, the use of $TiO_2$ in hydrogen photo production implies a significant waste of photon energy [9]. Returning to the energy diagram of Figure 1 we can argue that the energy loss is mainly due to the valence band, which is considerably more oxidizing compared with the reduction potential of the organic compounds considered until now.

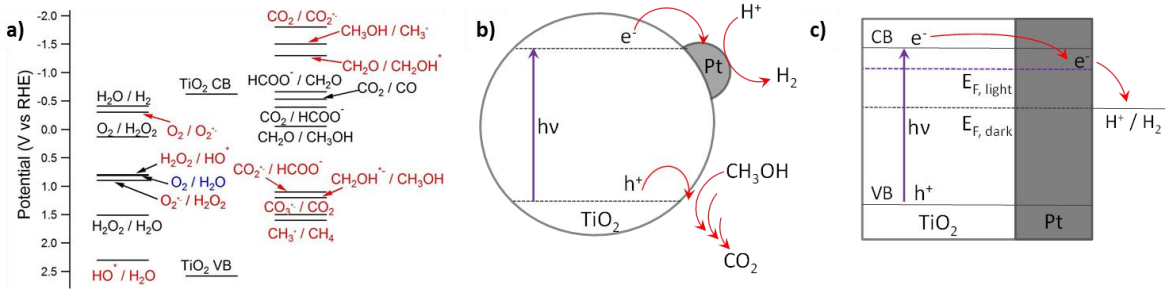


**Figure 2.** (**a**) Energy diagram showing the conduction and valence band potentials of $TiO_2$ anatase, C1 and water-related redox couples at pH 7 and 298 K [10–13] Monoelectronic couples are in red, bielectronic in black, the four-electron couple $O_2/H_2O$ is in blue. (**b**) Simplified pictorial scheme of the methanol reforming on a irradiated $Pt/TiO_2$ particle. (**c**) Photoinduced charge separation and charge distribution in $Pt/TiO_2$ nanocomposites. $E_{F,\,dark}$ and $E_{F,\,light}$ represent the pseudo-Fermi levels in the dark and under irradiation, respectively. Adapted with permission from [14]. Copyright 1979 American Chemical Society.

Conversely, the conduction band potential is very favorable, because it allows water reduction with a reasonable overpotential, which ensures a sufficient drive to carry out the reaction, without important losses. To minimize energy losses of photocatalytic reforming on $TiO_2$, hydrogen production should be coupled with the oxidation of recalcitrant compounds, when this reaction is kinetically limited or other strategies would not work, such as in the case of toxic compounds, aromatics, and antibiotics (scarcely removed in traditional wastewater treatment plants). Alternatively, the valorization of biomasses in remote regions could be another valuable and promising option, also because in that case $H_2/O_2$ separation could be ruled out [15].

### *1.2. History and Developments*

Usually the first example of water photosplitting is attributed to Fujishima and Honda and their 1972 paper published on Nature [16]. In their contribution rutile $TiO_2$ is used as a photoanode for the evolution of oxygen, while hydrogen evolution occurred at the platinum cathode. Their approach is therefore photoelectrochemical, because both irradiation and an external bias were required. There are only five references in their paper: the first is a 1910 paper [17], in which it was stated that water photolysis requires 190 nm or shorter wavelength light, while the other four are previous reports by

the same authors to a more specialized and narrow audience [18–21]. The small bibliography and the large rate of self-citation were due to the seminal nature of their report, but also to the smaller number of people, with different habits towards scientific publication, working in the field compared to nowadays. These two factors are still determining the reception of that work by the scientific community. Due to its seminal character the article received the first citation only two years later, but then interest rose up in the end of the decade and does not appear to slow down (Figure 3a) [22].

Considered as a whole, the literature concerning photoreforming on $TiO_2$ is increasing almost exponentially (Figure 3b) as water photosplitting publications are. Nevertheless, the sole increase of publication rate as a function of time in not significant, because of the unprecedented increase in the volume of the scientific literature occurred in the last decades. Indeed, even smallpox related publications show an increasing trend, even though the last recorded case dates back to 1977 [23]. More significantly, the increasing trend of water photosplitting publications is more similar to that recorded for lithium ion batteries, whereas hydrogen storage is showing a less steep increase since 8–10 years.

With the buildup of interest, the number of reports, experiments, and observations increased, empowering the understanding of the processes and the mechanisms involved. Compared to the beginning of the 1970s, nowadays we have a much vaster literature dealing with hydrogen production, heterogeneous photocatalysis and artificial photosynthesis. But even more than 50 years ago the first evidence that species such as $CN^-$, $I^-$ [20] $Br^-$, $Cl^-$, $Ce^{3+}$, $Mn^{2+}$ [24,25] and certain organics [26] could be oxidized by irradiated semiconductor slurries such as ZnO, $TiO_2$ and CdS thanks to charge carrier transfer [27] were already recorded. Moreover, Grätzel and coworkers sketched and demonstrated different strategies to evolve hydrogen in the presence (and also in the absence [28]) of $TiO_2$, even with visible light only [29,30]. The electron transfer from $TiO_2$ conduction band to $N_2$ was also reported [31]. In 1979, Bard published a comprehensive review [32] rationalizing the three possible approaches for the exploitation of electromagnetic energy with photoelectrochemical cells (PEC) based on semiconductors, namely photovoltaic, photosynthetic and photocatalytic. In photovoltaics, the goal is to obtain electricity from light, and the main development in the field came from dye-sensitized solar cells, which are regenerative photoelectrochemical cells capable of developing an electrical bias under irradiation and convert solar energy with 11.9% record efficiency [33].

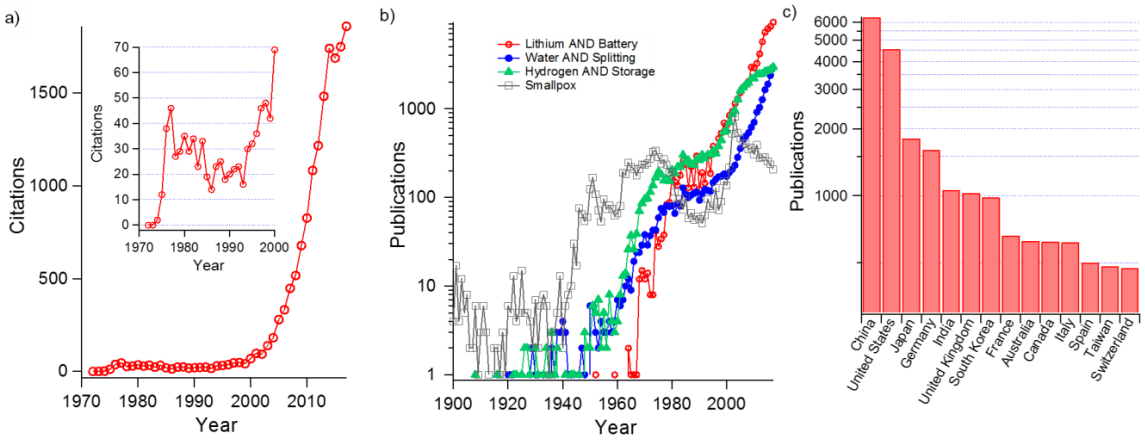


**Figure 3.** (**a**) Number of citations of the Fujishima and Honda 1972 article as a function of the time; inset: magnification of the 1970–2000 period. (**b**) Number of research article as a function of the publication year for lithium batteries, water splitting and hydrogen storage; smallpox is reported for comparison purposes. (**c**) Geographical distribution of the publications related to water splitting from 1920 to present. All the data were collected using the database Scopus®, Elsevier.

In the photosynthetic approach, light is converted into chemical energy, i.e., fuels, as in reaction (1), or, less evidently, in reactions (6), (9) and (10). Conversely, photoelectrochemical cells

for photocatalysis do not convert energy, but employ light to overcome energetic barriers and promote thermodynamically favored reactions, such as $CN^-$ oxidation, or reactions (7) and (8). Apart from providing many examples dating back to the 1950s, Bard outlined the similarities between semiconductor photoelectrodes and irradiated semiconducting slurries, which can, in principle, promote the same reactions. An irradiated semiconductor particle behaves as a short-circuited and miniaturized photoelectrochemical cell operating without bias. It is then evident that with the semiconductor slurry the prevention of recombination is an extremely important task to ensure high efficiency [32].

### *1.3. Mechanistic Considerations*

Since the earliest reports, it has been outlined that semiconductors such as ZnO or $TiO_2$ were able to oxidize organics and anions such as $I^-$ [20] and $CN^-$, and reducing $O_2$ to form hydrogen peroxide or water [34]. The addition of cocatalysts such as Pt and other noble metals improved the rates and allowed the evolution of hydrogen in anaerobic conditions. Other cocatalyst, such as $RuO_2$, allowed water oxidation to $O_2$ [35]. From these evidences, a first picture emerged regarding the mechanism of organics photoreforming on noble metal-modified semiconductors (Figure 2b). The photogenerated electron–hole couples are separated; the holes are transferred to the organics [36,37], while the electrons are captured by the noble metal, where they can promote water reduction and hydrogen evolution thanks to the low activation energy displayed by most noble metals and especially Pt [38,39]. At this stage is worth clarifying that the mechanisms of reaction in the dark, or under visible irradiation, where plasmonic resonance may be activated, could be radically different, as recently reviewed by Panayotov and Morris [40].

This pictorial unpolished mechanism is actually in good agreement with the experimental evidences collected during the years. It has been shown that hole trapping is a fast process, requiring less than 50 fs to happen, and that hole transfer to surface hydroxyl requires ≈250 ns, while in the presence of methanol the hole transfer significantly accelerates, being completed within 1 ns [41,42].

Conversely electron trapping is considerably slower, requiring ≈160 fs. Electron lifetime is in the order of the microsecond in vacuum or in the presence of water vapor, but it is extended to more than one second in the presence of methanol vapors. This demonstrates how electron and hole dynamics could be radically different when specific scavengers are introduced, and that their recombination, predominantly non-geminate and showing second order kinetics, strongly depends on these factors [43].

When $TiO_2$ is decorated with noble metal particles, electron trapping becomes at least 10–15 times faster compared with pristine $TiO_2$, whereas hole capture seems almost insensitive to noble metals [43]. This evidence is coherent with previous picture of electron capture by the metal where hydrogen evolution takes place (Figure 2b). A more refined treatment was carried out by Kamat and coworkers [14]: upon irradiation the Fermi level of the semiconductor is displaced towards more negative potential, because of the faster transfer of holes and to the accumulation of photoelectrons (Figure 2c). The Fermi level shift in the semiconductor causes an identical shift in the noble metal particles. If this shift is such that water reduction is triggered, hydrogen evolution will occur. This picture is coherent with the noble metal particle forming an ohmic contact with the semiconductor, rather than a Schottky junction, which should repel semiconductor electrons, especially in the case of noble metals, which have large work functions.

Because hydrogen evolution occurs on the noble metal, and because of the analogy between irradiated semiconductor slurries and photoelectrochemical cells, the study of the mechanism can take advantage from the enormous amount of work done by electrochemists on the hydrogen evolution reaction (HER) on metal electrodes (Figure 4).

HER is an archetypical reaction, in which two electrons and two protons are combined to form the simplest molecule $H_2$. The reaction requires two steps; the first is the Volmer step, the reductive adsorption or electrochemical discharge [44]:

$$H^+ + e^- + M\text{-}\square \rightarrow M\text{-}H$$

In which a proton from solution is reduced to become an adsorbed hydrogen atom on the metal surface. Of course, the Volmer step needs empty metal sites M-□ to proceed. At this point a bifurcation occurs, because the reaction may advance through the Tafel pathway, or H-H recombination:

$$2\ M\text{-}H \rightarrow H_2 + 2M\text{-}\square$$

Or through the Heyrovsky pathway, also known as reductive or electrochemical desorption [38]:

$$H^+ + e^- + M\text{-}H \rightarrow H_2 + M\text{-}\square$$

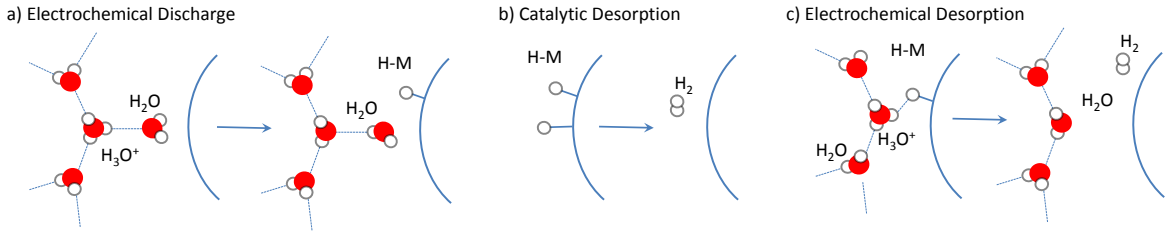


**Figure 4.** Electrochemical hydrogen evolution processes: (**a**) electrochemical discharge, or Volmer step; (**b**) catalytic desorption, or Tafel path; (**c**) electrochemical desorption, or Heyrovsky path. Adapted with permission from [38]. Copyright 1979 American Chemical Society.

The actual mechanism depends primarily on the metal. For example, on Pt, Pd and Rh HER proceeds mainly via the Tafel pathway. Interestingly, the same mechanistic features are found on Pt, Pd, and Rh decorated $TiO_2$ slurries, further confirming that hydrogen evolution is not only occurring on the metal cocatalyst, but also that the metal nanoparticles behave very similarly to their macroscopic electrodes counterparts. Moreover, poisoning the cocatalyst or in its absence HER is hindered, and the mechanism modified [38,45]. Even though common wisdom would suggest that the Volmer step could be limiting on metals with lower H adsorption energy, while on metals forming strong M-H bonds the mechanism could shift towards the Heyrovsky pathway, the actual mechanism depends on the electronic structure of the metal catalyst [46,47]. Apart from the chosen metal element, other parameters such as particle size, defectivity and exposed surfaces can therefore determine the overall rate. Moreover, the selection of the Tafel or the Heyrovsky pathway depends also on H surface coverage, which is potential dependent. While the working potential could be modulated if HER were carried out on a macroscopic electrode, it becomes uncontrolled, and usually unknown, in the case of a semiconductor slurry. Nevertheless, the Fermi level of the system will respond to changes in the identity and concentration of the organic substrate and of the incident photon flux. When the slurry is concentrated, the optical path through the reactor is long, the slurry illumination will not be uniform due to scattering, potentially leading to changes in relative $H_2$ reaction pathways along the optical path [48].

Hydrogen photoreforming is the result of the complex interplay among many elementary steps, such as light absorption, charge carrier recombination, hole transfer to substrate, which in turn can give current doubling or act as a recombination center, electron transfer from the semiconductor to the metal, proton reduction (electrochemical discharge) and hydrogen evolution on the metal, which occurs via catalytic or electrochemical desorption. In the case of readily oxidized organics giving current doubling, it is likely that the hydrogen evolution on the metal represents the rate-determining

step. Conversely, in the case of recalcitrant compounds, which can act as recombination centers, the rate determining step is likely to be on semiconductor side. Due to this variability, researchers devoted their efforts towards the improvement of both metal and semiconductor—and their coupling—as we will review in the next sections.

## 2. Shape Controlled $TiO_2$ Structures

While $H_2$ evolution occurs on the metal, charge separation and the oxidation semireaction efficiency are strongly related to $TiO_2$ morphology and surface texture.

Engineering the shapes of some materials to desirable morphologies was actively pursued. Many applications, such as heterogeneous catalysis, molecule adsorption, gas sensing and energy conversion are strongly dependent from surface atomic structures, which can be finely tailored by morphology control. Meaningful advancements in this area have been achieved [49–58].

Albeit a large amount of experimental and theoretical studies has been carried out on the characteristics of different surfaces of metal oxides [59–67], less attention has been paid on the dependence of the functional properties (reactivity, toxicity, osseointegration, etc.) on crystal surfaces exposed by metal oxides [68,69]. By tuning the ratio of different facets, the functional properties correspondingly change [70]. It is generally accepted that a surface with a high percentage of under-coordinated atoms has a greater reactivity [71–74]. A cooperative mechanism involving both favorable surface atomic structures and surface electronic structures has been recently proposed in order to explain the differences in reactivity [75]. Moreover, surfaces with higher reactivity usually have higher surface energy, so the possibility to obtain a pristine facet without the use of adsorbates was questioned [73], and upon removing the adsorbates the surface can reconstruct. However, reactive facets are highly desirable for improving and tuning functional properties. The shape evolution during the crystal growth is driven by the continue decrease of the total surface energy until the minimum surface energy point. Such process is conditioned by the presence of shape-controllers in the reaction environment.

The equilibrium shape of crystal structures can be predicted by using the Wulff construction [76], taking into account the surface energies of the crystal surfaces in the growth medium, if they are available. In the Wulff construction, surface energy minimization is used to optimize the composition of the crystal surface. The disadvantage is that only for clean crystal planes in vacuum are the surface energies available, and only in these conditions is the obtained equilibrium shape valid. The presence of liquid phases, electrolytes and adsorbates can change the equilibrium shape. The main $TiO_2$ polymorphs are anatase, rutile and brookite. All these three phases are constituted by $TiO_6$ octahedra, but in the case of anatase and rutile the crystal system is tetragonal, while for brookite is orthorhombic. The $TiO_6$ octahedra have different arrangements in the three polymorphs. Therefore, the surface terminations in various orientations are different, as well as the equilibrium morphologies of the crystals.

According to the Wulff construction, the equilibrium shape of the anatase is a lightly truncated bipyramid enclosed with eight trapezoidal {101} surfaces (>94%) and two top squares {001} surfaces, as shown in Figure 5A. Regarding rutile, the predicted equilibrium shape of a macroscopic crystal contains {110}, {100}, {001} and {011} faces (Figure 5B) [77]

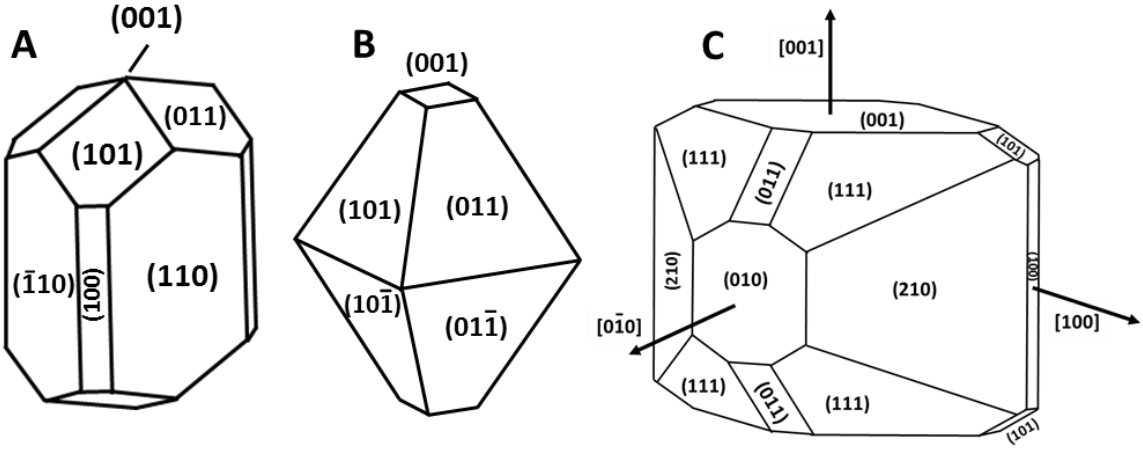


**Figure 5.** Equilibrium shape using Wulff construction for macroscopic crystals of rutile (**A**), anatase (**B**) and brookite (**C**). (**A** and **B**): adapted with permission from [60]. Copyright Elsevier, 2003. (**C**): adapted with permission from [78]. Copyright American Physical Society, 2007.

All the above predicted equilibrium shapes must be considered only in vacuum at 0 K [60]. By means of theoretical approaches, Barnard et al. found that the presence of water could influence the equilibrium shapes by changing the size and the aspect ratio of anatase and rutile [79]. Despite the high differences among vacuum conditions used in the calculations and hydrothermal/solvothermal conditions for crystal growth, the most stable facets predicted usually represent the largest fraction also in the real crystal surfaces.

## 3. Photocatalytic Hydrogen Production from Anatase $TiO_2$

In the last decade, several works have been devoted to the influence that the $TiO_2$ structure, particle size and morphology have on the charge carrier separation. The photocatalytic production of hydrogen can be performed using several $TiO_2$-based catalysts, with different morphologies and different exposed facets. In this Section, we will describe some $TiO_2$ anatase systems employed for $H_2$ evolution; in particular, the attention will be focused on the effect of the crystal morphology on the HER.

### *3.1. Effect of Crystal Shape and Structure*

The interaction of the $TiO_2$ crystals with the light can be changed modifying their size and shape in order to maximize the light absorption and the amounts of photogenerated charge carriers, in accordance with the Mie theory [80,81].

In 2011, Yun and coworkers [82] investigated the role of the $TiO_2$ nanoparticles shape in the photocatalytic hydrogen evolution. They compared nanospheres and nanorods using Pt as cocatalyst (1 wt %) and ethanol as sacrificial agent. They found that $TiO_2$ nanorods have higher UV photocatalytic activity due to a decreased probability of $e_{cb}^{-}/h_{vb}^{+}$ recombination. The authors, however, did not investigate the role of the different surfaces in their materials, probably responsible for the different electron hole recombination.

In 2011, Cho et al. [83], synthesized hierarchically branched $TiO_2$ nanorods for more efficient PEC devices, due to their large contact area, excellent light absorption and the conductive path for the charge carrier collection. They obtained three different nanostructured films, made of $TiO_2$ nanoparticles (NPs), nanorods (NRs) and branched nanorods (B-NRs). Under Xe lamp irradiation (880 W $m^{-2}$ total output, UV matched to AM 1.5G) NRs and B-NRs had higher performances when used in PEC devices, due to their enhanced light absorption and charge carriers transport. In particular, the higher surface area and the more effective charges separation in branched $TiO_2$ nanorods (B-NRs), resulted in an increased activity in comparison to simple nanorods (NRs).

Nanorods were studied also by Jiang et al. in 2013 [84]. They synthesized different immobilized anatase nanostructures from titanate nanowires by means of hydrothermal treatment. Changing the conditions of synthesis, two different structures were obtained: in neutral or acidic aqueous solution a chemical dehydration of titanate to anatase porous framework ($TiO_2$-PF) and nanowires ($TiO_2$-NW) occured, on the other hand mild alkaline conditions led to a dissolution-recrystallization mechanism, in this case nanorods were the final product with well-defined {010} and {101} surfaces ($TiO_2$-NR). Under solar simulated spectrum (41 W $m^{-2}$ in the UV), the authors found that the presence of the reactive {010} and {101} facets promoted the photocatalytic hydrogen evolution, overcoming the benefits of the intimate inter-particle contact of the hierarchical structures synthesized in neutral and acidic media.

Among different $TiO_2$ architectures, photonic crystal can also be exploited for studying the correlation between shape and photocatalytic activity. Photonic crystals are periodic optical nanostructure in which the refractive index varies periodically in the space. In this way they can affect the light propagation in the material [85]. If a given wavelength matches the lattice periodicity, a constructive interference of the reflected waves inside the material will be possible. At that wavelength, a complete reflection occurs and the light cannot propagate because of the photonic band gap. The group velocity of the light is strongly reduced at the edges of the photonic band gap (where it can propagate inside the crystal); therefore, the interaction with the material increases. This stronger interaction is called "slow light" or "slow photons" and can be exploited in several fields, including photocatalysis [86–89].

In 2015 Sordello and Minero [88] studied the hydrogen evolution rate from $TiO_2$ inverse opals (TIOs) and macroporous disordered (MP) structures that they synthesized using different polymeric sacrificial templates [88,90]. They used polymethylmethacrylate (PMMA) and polystyrene (PS) to obtain $TiO_2$ architectures with different pores size. The authors then compared the photocatalytic activity of the synthesized materials using Pt as cocatalyst and formate buffer (0.1 M) as hole scavenger. To study the effect of the photonic crystal slow photons, the hydrogen photoproduction tests were carried at two different irradiation wavelengths: at 365 nm, where the inverse opals studied were able to take advantage of the slow light, and 254 nm, where the contribution of the slow light was negligible. They concluded that under 254-nm irradiation, MP $TiO_2$ materials presented similar photoactivity compared to inverse opals, given the same polymer template. Conversely, at 365 nm, the slow photons effect induced a larger $H_2$ evolution for the inverse opals. Thanks to this approach they were able to prove that the rate increase stems from improved light absorption when photonic band gap edges and incident light emission maximum are matched and slow photons can be exploited. Without slow photons, inverse opals behave as disordered macroporous materials, confirming that charge transfer dynamics are not modified. The activities were also influenced by the chemical characteristics of the sacrificial polymer that controlled the crystalline phase of the $TiO_2$ materials. While PMMA induced the formation of anatase only, conversely, with PS a mixture of anatase and rutile was obtained.

The photonic crystal properties of $TiO_2$ nanotube arrays were exploited by Chiarello and coworkers [91] to enhance the photocatalytic hydrogen production under a polychromatic UV irradiation. Thin films of $TiO_2$ nanotube arrays on a Ti support were synthesized by electrochemical anodization. Figure 6 shows the vertically self-assembled nanotube arrays. The authors were able to linearly increase the inner diameter of the nanotubes and their growth rate increased with increasing applied voltage. From theoretical calculations, they demonstrated that the position and the width of the photonic band gap could be affected by three morphological characteristics of the nanotubes: (1) inner diameter, (2) wall thickness and (3) distance between pores. The possibility to change these characteristics by simply modifying the synthesis conditions, allowed tuning the photonic band gap and fitting it within the $TiO_2$ absorption band, red shifting the photoactivity threshold. This led to a > 50% increase of the $H_2$ evolution rate under polychromatic irradiation.

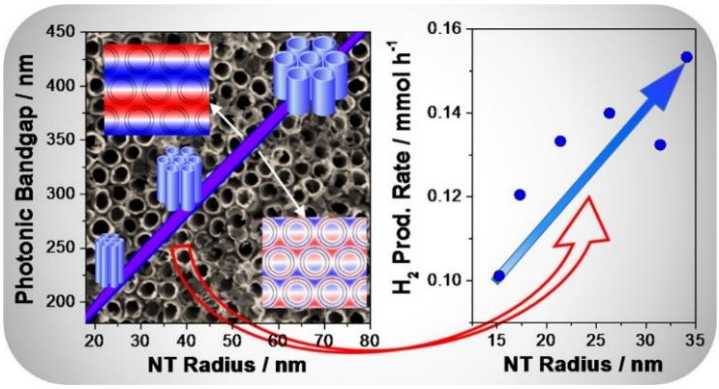


**Figure 6.** Dependence of the photonic band gap (**Left**) and $H_2$ production rate (**Right**) from the nanotubes inner radius. Reprinted with permission from [91]. Copyright © 2016 American Chemical Society.

### *3.2. Effect of Exposed Surfaces*

The strong dependence of the anatase nanoparticle photocatalytic activity on the typology of exposed surfaces, depend on its different reaction mechanisms occurring on different facets, due to their characteristic physicochemical properties [70]. In 2015 D'Arienzo et al. [92] studied the relationship between the different anatase surface and the $H_2$ generation yield in methanol photo-steam reforming under UV irradiation. They synthesized three different anatase crystals with shape nearly rectangular (RC), rhombic (R) and nanobar (NB) (Figure 7). They exposed {101}, {001} and, only for the RC, the {010} surfaces. They carried out Electronic Paramagnetic Resonance (EPR) experiments, correlating the amount of $Ti^{3+}$ (electron traps) with the $H_2$ evolution rate. They observed that the higher is the $Ti^{3+}$ EPR signal, the higher is the $H_2$ evolution rate. As we will report later, the {101} surface for anatase seems to be a reducing surface. Then, high exposition of this kind of facet should favor the formation of $Ti^{3+}$ centers under illumination and, therefore, better $H_2$ production.

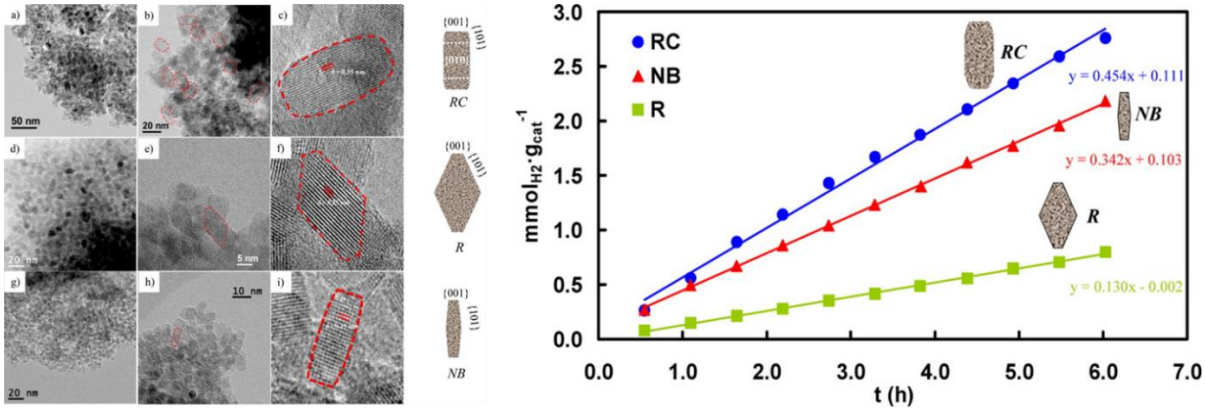


**Figure 7. Left**: Transmission Electron Microscopy (TEM) and High Resolution Transmission Electron Microscopy (HRTEM) images of shape-controlled $TiO_2$ nanocrystals produced by solvothermal synthesis. (**a**–**c**) Rectangular nanoparticles (RC); (**d**–**f**) rhombic nanocrystals (R); (**g**–**i**) nanobars (NB). **Right**: Hydrogen evolution during the photocatalytic steam reforming of methanol on shape-controlled anatase nanocrystals. Adapted with permission from [92]. Copyright © 2015 American Chemical Society.

From their results, the RC materials were the most active in methanol photoreforming and showed the largest density of $Ti^{3+}$ centers, however these materials had also the lowest {101} surface area, exposing preferentially the {010} surface. This points out that the $H_2$ production cannot be related only to the extension of the reductive {101} surface, but also to presence of the {010} facet seems to

play a role. The authors suggested the presence of a "surface hetero-junction" between the {101}, {010} and {001} facets which drives the electrons photogenerated on the {001} not just toward the {101}, but also to the {010}, favoring the charge separation. The idea of "surface hetero-junction" is one of the most employed concepts for explaining the synergistic effect of the different surfaces of $TiO_2$ nanocrystals [93,94]. Figure 8 reports the charge transfer process using energy level diagram of the "surface hetero-junction" between facets {101} and {001} of $TiO_2$ anatase.

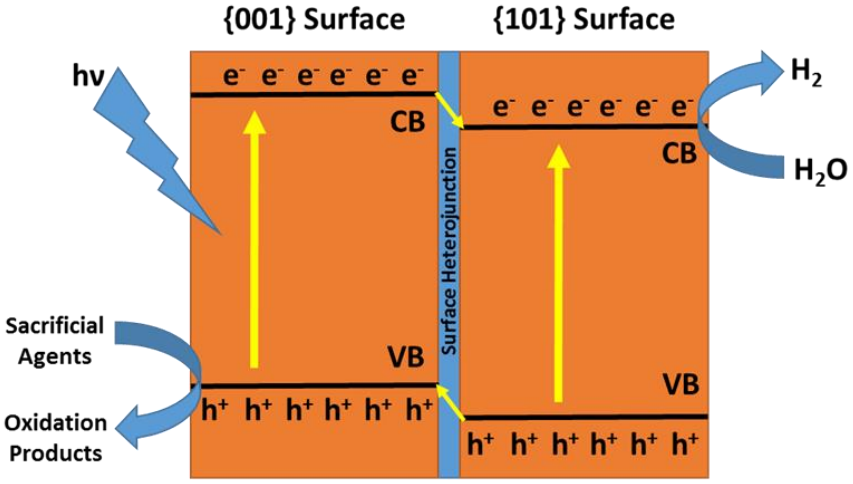


**Figure 8.** Energy-level diagram and charge carriers transfer process of the "surface hetero-junction" between facets {101} and {001} of $TiO_2$ anatase under UV irradiation.

The importance of the exposed surfaces is highlighted also in the recent paper of Liu, Page and coworkers [95]. They synthesized anatase NPs with different relative amounts of {101} and {001} surfaces. They obtained that the catalyst with an intermediate amount of the {101} and {001} surfaces, normalizing for the SSA, showed the best UV photocatalytic activity in the $H_2$ production from a methanol solution (Figure 9). They concluded that a synergistic effect may exist between {001} and {101} facets.

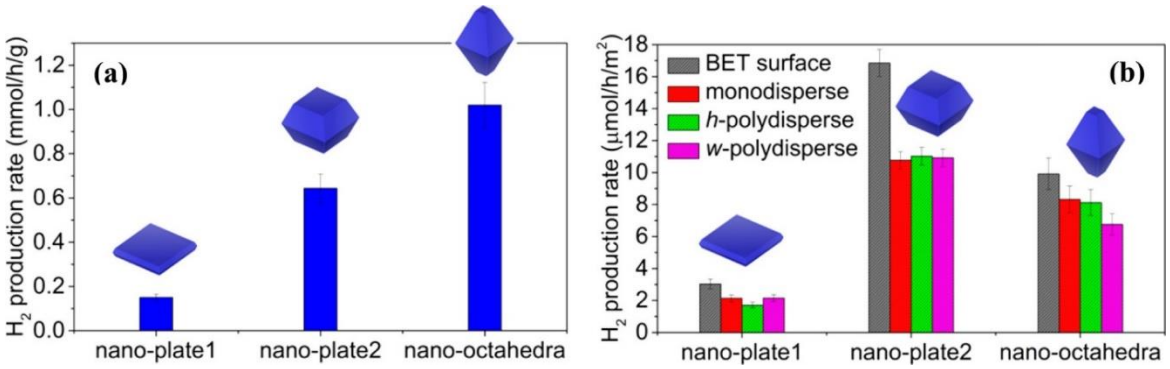


**Figure 9.** (**a**) Mass and (**b**) surface normalized photocatalytic hydrogen evolution rate of three anatase $TiO_2$ nanocrystals with different {001} to {101} facet ratios. Reprinted with permission from [95]. Copyright © 2017 American Chemical Society.

In 2012 Gordon et al. [49] used $TiF_4$ as precursor in the synthesis of anatase nanocrystals to produce HF in situ for controlling the crystal shape. Through the change of the ratio of $TiF_4$ precursor in combination with $TiCl_4$ and the type of surfactant (oleylamine or octadecanol), a tunability of the titania shape based on bipyramidal geometry was demonstrated (Figure 10). The percentage of {101} and {001} facets was therefore well controlled and depended on the amount of HF released during the reaction, resulting in samples where F was still present on the surface. Then, treatment with

NaOH exchanged the fluorides at the surface with OH groups. The materials were then tested for $H_2$ production in the presence of methanol as sacrificial agent and photodeposited Pt as cocatalyst under simulated solar light. The results showed that the samples with higher content of {101} facets were better than {001} for this particular reaction, both with and without fluorine on the surface. This clearly demonstrates the importance of the presence of the {101} to have efficient reductive processes.

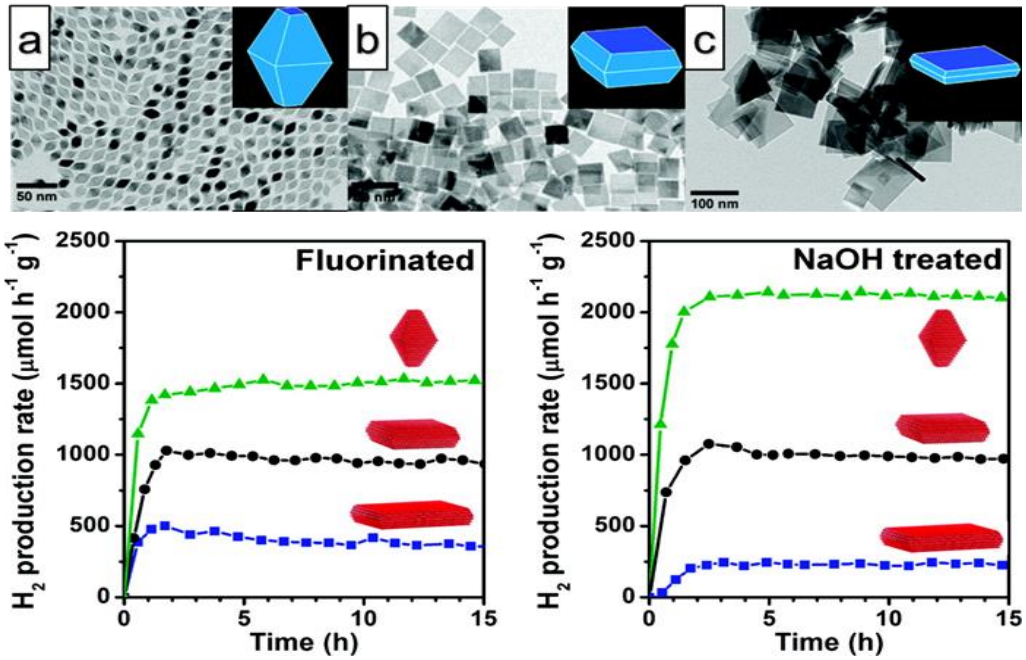


**Figure 10. Top**: TEM images of $TiO_2$ nanocrystals synthesized (**a**–**c**). **Bottom**: $H_2$ production rate over fluorinated and NaOH-treated materials. Adapted with permission from [49]. Copyright © 2012 American Chemical Society.

The photocatalytic production of hydrogen from methanol steam reforming was also investigated over a series of fluorinated $Pt/TiO_2$ samples (F for O nominal molar substitution ranging from 5 to 15%) synthesized by flame spray pyrolysis by Chiarello et al. in a work published in 2014 [96]. A substitution lower than 10% led to an increase of surface hydroxylation which favored an indirect hydroxyl mediated mechanism, with the consequent increase of hydrogen production rate. Conversely, fluorination > 10% introduced an excess of bulk structural defects that can act as electron–hole recombination centers. Moreover, an excess of fluorination increases the F-induced surface electronegativity, inhibiting CB electron transfer. Both these effects led to lower hydrogen production rate under UV irradiation.

The effect of the nanoparticles shape and the surface fluorination were investigated by Yu and coworkers in 2010 [97], investigating the hydrogen production over $Pt/TiO_2$ nanosheets that largely exposed {001} facets. They prepared anatase nanosheets by acidic hydrolysis of Ti(IV) butoxide using hydrofluoric acid as capping agent. A part of the obtained nanoparticles was then cleaned with diluted 0.1 M NaOH solution in order to remove the surface fluorides. To investigate the influence of the shape, the same synthesis procedure was repeated but replacing the hydrofluoric acid with the same volume of distilled water. Pt nanoparticles were photodeposited from a 0.26 mM $H_2PtCl_6$ solution in order to obtain a final weight ratio of Pt to Ti of 2%. The fluorinated $TiO_2$ material presented higher photocatalytic activity than the other two materials, due to the synergistic effect of fluorination (reduction of the charge carriers recombination rate) and exposed {001} facets. The higher reactivity of the {001} facet is in contrast compared with most of the works published in the last few years. For example, Pan et al. [75] synthesized anatase microcrystals with three different morphologies and different percentages of {101}, {010} and {001} surfaces. The hydrogen evolution on the samples

was estimated from methanol (10%) photoreforming using 1 wt % Pt cocatalyst under Xe arc lamp irradiation. The authors found that the presence of fluorides (derived from synthesis conditions) is deleterious for the photoreduction of $H_2$, especially for the surfaces {101} and {010}, counteracting the different facets terminations. After removal of the capping agent (2 h 600 °C in air), the F-free surfaces presented different behaviors, with a new photoreactivity order ({010} > {101} > {001}).

Ohtani and coworkers [98], in 2009, described a synthetic procedure to obtain decahedral anatase nanoparticles through a gas-phase reaction using $TiCl_4$ as precursor and with a rapid heating and quenching. The obtained material showed ≈40% of {001} surface, with a BET specific surface area of 9.4 $m^2$ $g^{-1}$. The activity of the material was evaluated on methanol photoreforming using UV light and Pt (2 wt %) as cocatalyst, deposited on the semiconductor from two different precursors: $H_2PtCl_6$ or $[Pt(NH_3)_4]Cl_2$. The authors compared the synthesized nanoparticles and the commercial $TiO_2$ P25 material. Due to the low density of crystalline defects, the decahedral nanoparticles were more reactive than $TiO_2$ P25 in the hydrogen evolution from methanol solution.

### *3.3. Effect of the Cocatalyst*

Numerous are the cocatalysts coupled with $TiO_2$ proposed to maximize the rate of electron transfer to $H^+$ and consequently increase the overall efficiency of both water photosplitting and photoreforming. The most efficient cocatalysts are noble metals such as Pt, Au and Pd [99–108], but also materials based on Ag, Rh, Ni, Mn, Ru, Cr, and Co were proposed [109–115]. Furthermore, different carbon-based materials (e.g., graphene, graphene oxide, single-wall and multi-wall carbon nanotubes, carbon nanocones, graphitic-$C_3N_4$ ... ) [101,104,116–121] have been recently reported as active materials to (*i*) delocalize the electron in the conduction band thanks to their proper work functions (significantly lower than the CB of the titania), (*ii*) decrease the overpotentials for the proton reduction. An overall agreement on the role of the carbonaceous phase during the photocatalytic process under irradiated hybrid systems has not been reached yet. One reason is that different materials, or the same materials synthesized with different procedures, can have significantly different electronic structures. The partitioning of the photogenerated charges between the semiconductor and the carbon-based material is strongly affected by their electronic properties (especially in terms of energetic positioning of the bands) and, consequently, this point is not easy to be rationalized comparing the photocatalytic behavior of materials only seemingly similar. An agreement on the role of the carbonaceous phase (graphene, grapheme oxide, reduced-GO ... ) has been reached for the photocatalytic degradation of dyes on hybrid systems. In this case a dye-sensitized degradation mechanism seems to be active: an electron promoted in the LUMO of the dye—as a consequence of the absorption of a visible photon—is rapidly delocalized toward the carbonaceous phase—where the dye is usually strongly adsorbed—and here it reacts with the dissolved oxygen to generate the radical $O_2^{\bullet-}/HO_2^{\bullet}$. Then the oxidized dye can autonomously evolve forming stable or transients byproducts [122,123]. Pastrana-Martínez et al. investigated the photocatalyzed degradation of the colorless diphenhydramine and the organic dye methyl orange and demonstrated that under visible irradiation the self-oxidation of the visible-absorbing species is the dominant mechanism [124]. Under UV irradiation the transfer of the charged carriers between the two solid phases and between the hybrid catalyst and the reactants in solutions (e.g., $H_2O$ to be reduced for the production of $H_2$ or a sacrificial organic compound in the case of carbon photoreforming) has not been totally clarified. It was suggested by Minella et al. that on UV-irradiated $TiO_2$/rGO hybrids, it is possible both the electron transfer from exited states of rGO onto the titania conduction band and the hole transfer from the $TiO_2$ to the carbonaceous phase where the sacrificial substrate is adsorbed and oxidized, if and only if the HOMO of the substrate has a less positive redox potential (higher energy) than the empty state of excited rGO [123]. Similarly, Hu and Tang suggested that during the photocatalytic transformation of phenol on visible irradiated hybrids composed of rGO and titanate nanotubes (TNTs), the photogenerated electrons in the graphene can be injected into the TNTs conduction bands although the presence of a Schottky barrier. In this case the degradation of phenol under visible

irradiation was related to the indirect formation of highly reactive hydroxyl radical mediated by the formation of $O_2^{\bullet-}/HO_2^{\bullet}$ as also suggested by Qianqian et al. [125]. The kinetics of transfer of electrons from high-energy rGO states toward the $TiO_2$ are characterized by kinetics in the 0.1–0.2 ps range. The ab-initio calculations carried out by Long et al. [126] suggested that the electron transfer process can occur from photoexcited states of graphene sheets without defects onto the titania surface with a non-adiabatic mechanism. On the contrary, the EIS evidences reported by Wang et al. investigating the $TiO_2$-rGO/electrolyte interface suggested that electrons in the $TiO_2$ conduction bands can be transferred onto rGO sheets, but also that the holes in the valence bands can move toward the rGO phase promoting an effective degradation of adsorbed molecules [127]. The main conclusion from the analysis of the scientific literature on this topic (see as an example the recent reviews [128,129]) is that it is quite difficult to generalize because the numerous modifications of the synthesis and the intrinsic differences between materials only seemingly similar can affect abruptly their photocatalytic performance, the electronic structures of the hybrids and—ultimately—the dynamics of the photogenerated charge carries.

Recently, numerous Cu-containing species (Cu [105,130,131], $Cu_2O$ [132], $CuO_x$ [133], CuO [134], $Cu(OH)_2$ [135] and $Cu_2(OH)_2CO_3$ [136,137]) showed relatively high photocatalytic rate, even if a complete agreement on the operative electron transfer mechanism has not been reached yet. The complex redox speciation of the copper-based materials seems to force the $e^-_{cb}$ of $TiO_2$ to be delocalized on the cocatalyst and here react to produce hydrogen. The role of Pt and Au in the photoreforming of methanol under irradiated Pt- and Au-supported titania was investigated by Naldoni and coworkers [100] by in-situ electron spin resonance (ESR) spectroscopy. Both the nature of the cocatalyst and its loading strongly affected the $H_2$ evolution rate and the nature and relative concentration of the byproducts of the methanol oxidation. The best performance was reported for Pt-$TiO_2$ and this was attributed to the better ability of Pt to act as electron sink with compared with Au. This was directly demonstrated evaluating the concentration of the $Ti^{+3}$ paramagnetic sites under irradiation that followed the order: pristine $TiO_2$ > Au-$TiO_2$ > Pt-$TiO_2$. The electrons photopromoted were better delocalized on the metal phase—especially with platinum—giving a lower concentration of $Ti^{+3}$ species. Interestingly, in the adopted experimental conditions the oxidation of methanol was only partial and significant amounts of formaldehyde were reported (see Figure 11).

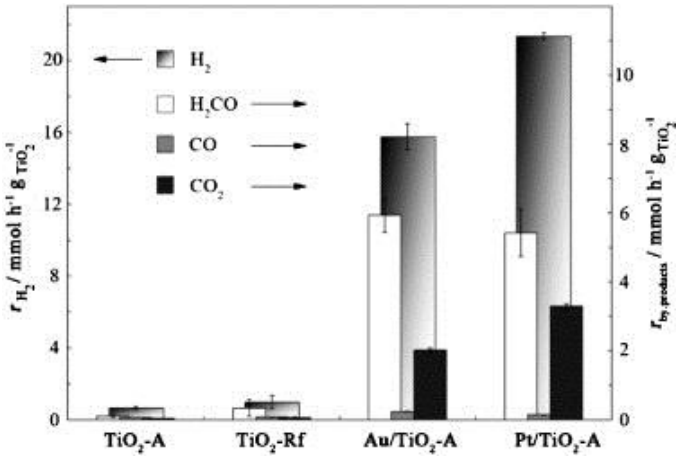


**Figure 11.** Hydrogen, formaldehyde, carbon monoxide and carbon dioxide production rates on 4 different $TiO_2$-based photocatalysts. $TiO_2$-A and $TiO_2$-Rf are pristine nanometric $TiO_2$, while Au/$TiO_2$-A and Pt/$TiO_2$-A are as $TiO_2$-A but decorated with nanometric particles of Au and Pt, respectively. Reprinted with permission from [100]. Copyright Elsevier, 2013.

In water photosplitting the back reaction giving water from the evolved products ($H_2$ and $O_2$) has to be limited to maximize the quantum yield of the process. As an example, Au, NiO and $RuO_2$ are suitable cocatalysts also because the back reaction hardly proceeds because the reductive and oxidative sites on these catalytic systems are spatially separated. Interestingly, a suitable cocatalyst for

the $H_2$ evolution from water on irradiated semiconductor—not only $TiO_2$—is NiO, which is usually formed by $H_2$ reduction of islands of nickel oxide on the semiconductor photocatalyst surface and subsequent partially oxidation with $O_2$ to form biphasic Ni/NiO layer structure. This structure is usually denoted as $NiO_x$ and is able to favor the charge carrier separation promoting the evolution of $H_2$ on the surface of the cocatalyst (in aqueous suspension mainly formed by $Ni(OH)_2$) and avoiding the back reaction between $H_2$ and $O_2$ being the oxygen evolution sites spatially separated from the cathodic sites. For further information on the electrochemical behavior of NiO, please refer to [138].

The chemical nature of the cocatalysts is as important as their structural features and consequently the same material structured in different nanometric forms can have significantly different efficiency. An in-depth analysis of the most investigated and the most promising cocatalysts is far from the scope of this review. To deepen this topic, please refer to [139,140].

### *3.4. Effect of the Sacrificial Agent*

The increment of the $H_2$ photoproduction rate can be obtained choosing properly the hole scavenger. Despite of the huge works on the use of methanol as a reductant, its implementation cannot at this stage be considered a green technology, because no green process for the production of methanol is really operative and its production is mainly carried out through the catalytic conversion of synthesis gas to methanol in fixed bed reactor [141]. However, methanol is an ideal substrate for the investigation of the process and this justifies the efforts carried out to clarify the operative mechanism. Particularly, the oxidation of gaseous methanol to $CO_2$ involves successive oxidative steps comprising both $^{\cdot}OH$ mediated oxidation and direct hole transfer to the adsorbed methanol with the production of formaldehyde, formic acid and $CO_2$ [45].

Bahruji and coworkers investigated the photocatalytic reforming of a variety of oxygenates compounds under UV irradiated $Pd/TiO_2$ providing insight into the effect of molecular structure on the reaction kinetics [108]. The rate of $H_2$ production with the different hole scavengers is reported in Figure 12. From these experimental evidences some general rules were proposed to achieve high $H_2$ production rate from the reforming of alcohols over Pd -$TiO_2$ catalysts: the alcohol must have a hydrogen in the adjacent position ($\alpha$) with respect to the oxygen atom (few $H_2$ production was observed in the presence of acetic acid or acetone); the primary alcohols release $CO_2$ for decarbonylation and the related alkyl groups yields the corresponding alkanes (with the clear exception of methanol) and the carbon in the methylene groups finally undergoes complete oxidation to yield $CO_2$. Bowker et al. [142] underlined the essential role that the hydroxyl groups in the organic reductant have to achieve effective photoreforming, being chemicals such as alkanes and alkenes inactive.

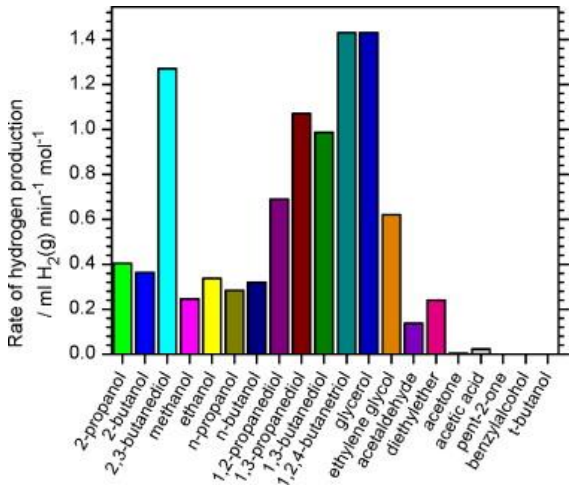


**Figure 12.** Hydrogen evolution rates under irradiated $Pd/TiO_2$ catalyst in the presence of different alcohols. Reprinted with permission from [102]. Copyright Elsevier, 2011.

The mechanism of reaction of organic substrates in photocatalytic condition has been in-depth investigated since from the seminal works on photocatalysis [143–148]. The fundamentals of semiconductor photocatalysis are now well understood and the presence of a complex network of oxidative paths involving both direct and mediated electron transfer at different reactive sites well accepted. Moreover, catalysts with different surface properties can promote transformation in which the relative weight of the different paths is different, with the consequent production of different byproducts [149,150]. Furthermore, the photocatalytic reactivity is dramatically influenced by both the intrinsic (crystallographic phase, surface defects, band potentials, doping, etc.) and extrinsic (pH, composition of the solution, presence complexing ions, etc.) properties of the photocatalyst in a manner often difficult to be rationalized. Even if rationalized with some difficulties, also the optical properties (absorption vs scattering) of the photocatalyst affects dramatically the ability of a semiconductor to harvest the radiation and consequently to promote the photocatalytic process (e.g., the photocatalytic reforming of organic compounds) [48,151].

As underlined above, photoreforming can be really considered a green technology only if the organic compounds used as sacrificial agents are wastes or they are produced through $CO_2$ neutral processes. In this light the best candidates and the most studied substrates are:

(1) Ethanol, which is produced in a large number of fermentation processes of second-generation biomasses, as well as by the transformation of cellulose and lignocellulose [152]. The mechanism of reaction for the ethanol photoreforming was investigated on $Pt/TiO_2$ catalyst. The mechanism proposed followed the scheme described above where protons are reduced by electrons cumulating into Pt particles, while the chemisorbed or physisorbed ethanol is stepwise oxidized by holes [153]. The stepwise oxidation of the substrate gives predominantly acetaldehyde, acetic acid and $CO_2$, but also compounds with larger number of carbon atoms, such as acetone and 2-butenal. 2-butenal (crotonaldehyde) can be formed by the aldol condensation of two acetaldehyde molecules or through the formation of the $^{\cdot}CH_3CHO$ radicals. In a similar way a possible path for the production of acetone is the reaction of acetaldehyde (or acetic acid) with $^{\cdot}CH_3$ radicals [154]. The accumulation of byproducts can give a partial poisoning of the catalyst with its progressive deactivation [155].

(2) Glycerol, which is the main byproduct of the biodiesel industry, is alternatively produced through the sorbitol hydrogenolysis or the fermentation of glucose [156,157]. Considering that (*i*) the total reforming of one molecule of glycerol gives 7 molecules of $H_2$ and (*ii*) the raw glycerol obtained as byproduct of the biodiesel industry is a complex mixture—containing methanol, water, inorganic salts, free fatty acids, triglycerides, and methyl esters—that requires expensive treatments to be purified, the energetic valorization of glycerol is a very promising path. The mechanism of transformation of glycerol on bare $TiO_2$ was investigated by Minero et al. [140] Glyceraldehyde (GAD), dihydroxyacetone (DHA), formaldehyde (FORM) and glycolaldehyde (GLY) were identified as the main byproducts obtained through two different reaction paths. GAD and DHA are the products formed from the OH radical mediated oxidation, while FORM and GLY are produced through a direct electron transfer (hole transfer from $TiO_2$ to the chemisorbed glycerol). Interestingly, the ratio between the produced byproducts is strongly affected by the surface properties of the catalyst. The direct hole transfer is favored on catalysts with more defective surfaces able to strongly adsorb the substrate on the more defective (and more reactive) sites.

(3) Glucose, and other simple or complex sugar, which are mainly obtained from the degradation of cellulose materials [158,159]. The photoreforming of sugars, starches and cellulose was demonstrated for the first time on the ternary photocatalyst $RuO_2/TiO_2/Pt$ [155]. As reported above, these substrates are ideal candidates to promote an efficient photoreforming because of the presence in the sugar molecules of numerous hydroxyl groups with hydrogen atom in α position. The more complex the carbohydrates, the lower is the efficiency. Fu and coworkers investigated systematically the glucose photoreforming under irradiated $TiO_2$ decorated with different metal

cocatalysts in the absence of oxygen, and observed the following reaction rate: Pd > Pt > Au ≈ Rh > Ag ≈ Ru. The presence of $O_2$—as expected—and the decrement of the pH inhibited the hydrogen production [159]. Recently, Kennedy et al. compared the hydrogen production with C2-C5 polyols, cyclic alcohols and mono and di-saccharides under irradiated Pd-$TiO_2$. For the compounds in the first class the hydrogen evolution rate is directly related to the number of OH groups and the availability of hydrogen atoms in α position to the hydroxyl. This rule is not followed by the cyclic alcohols and especially sugar (glucose, fructose and sucrose). For the reforming of cyclic alcohols it was also observed the dehydrogenation and decarbonylation of α CC bond [107].

Furthermore, other organic compounds were investigated such as diols, superior alcohols and polysaccharides.

Caravaca and coworkers focused on the photoreforming of cellulose on a $TiO_2$ catalyst loaded with both Pt and Ni with UV irradiation. In the presence of both cocatalysts the photoreforming occurred with significant hydrogen production. The first step of the process was the (photo)hydrolysis of cellulose into glucose, which was then easily oxidized thanks to the highly hydroxilated structure. These results demonstrated the possible production of hydrogen directly from the main components of the biomass (the cellulose) without any intermediate steps [114]. To give more insights into the features of the photocatalytic reforming process of the above cited compounds, please refer to the excellent review by Cargnello et al. [160] and Rossetti [161].

An alternative approach is to consider the waste of the industrial or civil Waste Water Treatment Plants (WWTPs) as potential source of carbon to be photocatalytically reformed. In this line, Speltini et al. investigated the photocatalytic production of hydrogen in the presence of swine sewage as sacrificial agent observing significant evolution of hydrogen on Pt-$TiO_2$ upon UV-A and solar light [162]. Moreover, Liu et al. described the contemporary degradation of waste activated sludge and the simultaneous production of hydrogen in a fluidized tubular photocatalytic reactor [163].

## 4. Environmental Implications

An in-depth evaluation of the environmental impacts of a new technology—especially in the energetic field—is always mandatory to avoid that its employment causes severe perturbations of the fragile environmental equilibria. In this light, the lessons from the past (e.g., the depletion of stratospheric ozone as a consequence of the release of chlorofluorocarbons or the dramatic decrement of biodiversity as a consequence of the overuse of pesticide in vast area of the Earth) should drive the decisions related to the implementation of new technologies in our society. This has a general validity, but it is especially true for the technologies related to a massive market such as that of the energy.

The first environmental consideration about the processes for the production of hydrogen through photochemically driven and $TiO_2$-based technologies described and commented above, should start from the abundance of the elements on the Earth's crust. Titanium is an abundant element (with an average concentration in the continental crust equals to 4010 ppm [164]). Its availability does not represent an obstacle for a massive employment of titanium dioxide-based technologies. However, we have previously underlined the essential role of cocatalysts to significantly increase the rate of $H_2$ production, low on pristine $TiO_2$. In this light, as the abundance of the most investigated cocatalysts, namely Au, Pt and Pd, is very scarce (0.25, 0.4 and 0.4 ppb, respectively [164]) and a vast application of a technology based on these rare elements could not be envisaged, also because these new applications would be in competition with their more traditional industrial uses. The employment of cocatalysts based on copper seems more plausible thanks to its average higher abundance (25 ppm [164]). Clearly, the use of carbon-based cocatalyst or hybrid organic/inorganic structures does not have any hindrance from the point of view of the elemental abundance. In this case, the attention must be paid on the technologies employed for the production of innovative, complex and nano-engineered organic structures. A careful evaluation of the environmental impact of the production of these materials (e.g., graphene-like materials, CNTs, fullerenes . . . ) in terms of both energy request and environmental

impact of their production process must be carried out. In this light, the evaluation of the overall process based on Life Cycle Assessment (LCA) is mandatory to really evaluate environmental merits and demerits of a technology. As an example, the actual processes for the production of significant amount of graphene-like structures are mainly based on a top-down approach starting from graphite. The strong oxidation of the original graphite is carried out through modifications of the original Hummer's method [165,166] that allows the production of huge amount of graphene oxide, but through a process heavy from the environmental point of view (e.g., use of concentrated mineral acids and oxidants).

Furthermore, the carbon photoreforming through the use of sacrificial agents (see Section 3.4) cannot be considered an *a priori* green technology because the nature of the sacrificial agents and the process used to produce them can modify enormously the overall green metrics of the process. The production of plants with pure energetic aims must be totally avoided not to compete with the food production. Furthermore, the sacrificial hole scavengers should be either an organic waste of primary industrial processes (e.g., the glycerol that is a byproduct of the biodiesel industry) or compounds produced from wastes of low-energy demanding processes and/or from other production chains. In all the cases, the overall life cycle for the hydrogen production technology investigated must be compared with that of the electrochemical production of hydrogen through the electrolysis of water that has yield almost quantitative (the electro-splitting of water on platinized anodes reach $\eta \geq 90\%$). This process, if based on the use of renewable energy sources, could have a dramatically low environmental impact.

Even though hydrogen production from irradiated semiconductors will probably have a marginal importance in the short- to medium-term, other technologies could be the drivers to the eventual transition toward a hydrogen-based economy. This scenario must be carefully evaluated taking into account not only the physical limits of our Planet, but also the complex network of reactions at the basis of the terrestrial equilibria. These could be perturbed by a significant hydrogen leakage during its production, transportation and use [167]. In this respect, the main environmental concerns are the possible impacts on the stratospheric ozone and its role as indirect greenhouse gas [168,169].

## 5. Conclusions

From the prior discussion, we can summarize the progresses of the research on photocatalytic $H_2$ production on $TiO_2$ into these three major areas:

1. $TiO_2$ crystal morphology:
    a. *Structuration.* The crystal shape and size can be modulated in order to maximize the light absorption and, therefore, the charge carrier density under irradiation. The same effect can be achieved with photonic crystal structures, which can increase the performance of $TiO_2$, as discussed in the Section 3.1.
    b. *Exposed Facets.* Besides light absorption, morphology can also decrease the recombination of the charge carriers, accelerating their interfacial transfer. This was highlighted by several works, demonstrating the different behavior of the exposed facets for $TiO_2$ anatase and rutile. In the case of hydrogen evolution on anatase, the surface {101} has a prominent role due to his reductive nature. In the presence of a cocatalyst as Pt, the higher is the amount of the {101} surface the higher is the rate of $H_2$ photoproduction. Conversely, on pristine $TiO_2$ surface, a synergistic effect results between the different surfaces of anatase crystals, indicating the formation of a "surface heterojunction" that increases the efficiency of nanoparticles exposing considerable amount of oxidative surface.
2. Cocatalyst. The role of the cocatalyst is crucial for improving the $TiO_2$ activity in the $H_2$ photoproduction. The common characteristics of a good cocatalyst in HER are the ability to drain photoelectrons from the conduction band and then decrease the required overpotential for reducing the proton. Noble metals are still in a predominant position, and especially Pt shows

the best activity, followed by Pd, while Au and Ag perform relatively worse. Other metals, such as Rh, Ni, Mn, Ru, Cr and Co, were recently proposed. The emergence of cheaper alternatives, such as Cu and carbonaceous materials (graphene, $C_3N_4$, etc.) could substantially decrease the costs of the $H_2$ production, especially in the prospect of large-scale production.

3. Substrates and Sacrificial Agents: usually, the role of the hole scavenger goes into the background compared to the reductive part in photocatalytic reforming. However, the sacrificial agent largely affects the $H_2$ photoproduction. While a wide range of alcohols (methanol, ethanol, propanol, etc.) can be exploited mainly for research purposes, to better understand the mechanisms involved in the process, the coupling with biomass-derived substrates, such as glycerol, glucose and sugars, or recalcitrant pollutants, could be a useful way for producing $H_2$ in a greener manner and to fully exploit the positive valence band potential of $TiO_2$ and other wide band gap semiconductors.

**Author Contributions:** F.S., M.M. and F.P. contributed equally to the conceptualization, writing and editing of the Review. V.M. and C.M. contributed as supervisors and reviewers.

**Funding:** F.P., V.M. and F.S. acknowledge funding from Regione Piemonte, Bando LR34/2004—"Studio preliminare e sviluppo di soluzioni innovative di materiali d'attrito in ambito Automotive". M.M. and C.M. acknowledge the financial support from project "Ricerca Locale", University of Torino.

**Conflicts of Interest:** The authors declare no conflict of interest.

## References

1. Smil, V. *Energy Transitions: Global and National Perspectives*, 2nd ed.; ABC-CLIO: Santa Barbara, CA, USA, 2017.
2. Raupach, M.R.; Davis, S.J.; Peters, G.P.; Andrew, R.M.; Canadell, J.G.; Ciais, P.; Friedlingstein, P.; Jotzo, F.; van Vuuren, D.P.; Le Quéré, C. Sharing a quota on cumulative carbon emissions. *Nat. Clim. Chang.* **2014**, *4*, 873. [CrossRef]
3. Meinshausen, M.; Meinshausen, N.; Hare, W.; Raper, S.C.B.; Frieler, K.; Knutti, R.; Frame, D.J.; Allen, M.R. Greenhouse-gas emission targets for limiting global warming to 2 °C. *Nature* **2009**, *458*, 1158. [CrossRef] [PubMed]
4. Yen Kheng, T. Review of Energy Harvesting Technologies for Sustainable WSN. In *Sustainable Wireless Sensor Networks*; Sanjib Kumar Panda, E.D.W.S.E.D.Y.K.T., Ed.; Charpter 2; IntechOpen: Rijeka, Croatia, 2010.
5. Armaroli, N.; Balzani, V. The Hydrogen Issue. *ChemSusChem* **2011**, *4*, 21–36. [CrossRef] [PubMed]
6. Bowker, M. Photocatalytic Hydrogen Production and Oxygenate Photoreforming. *Catal. Lett.* **2012**, *142*, 923–929. [CrossRef]
7. Bockris, J. *Modern Electrochemistry 1, 2A, and 2B*; Springer: New York, NY, USA, 2007; p. 2158.
8. Hammes, G.G.; Hammes-Schiffer, S. *Physical Chemistry for the Biological Sciences*, 2nd ed.; John Wiley & Sons, Inc.: Hoboken, NJ, USA, 2015.
9. Noufi, R.N.; Kohl, P.A.; Bard, A.J. Semiconductor Electrodes XV. Photoelectrochemical Cells with Mixed Polycrystalline n-Type CdS - CdSe Electrodes. *J. Electrochem. Soc.* **1978**, *125*, 375–379. [CrossRef]
10. Fujishima, A.; Zhang, X.; Tryk, D.A. $TiO_2$ photocatalysis and related surface phenomena. *Surf. Sci. Rep.* **2008**, *63*, 515–582. [CrossRef]
11. Grätzel, M. Photoelectrochemical Cells. *Nature* **2001**, *414*, 338–344. [CrossRef]
12. Koppenol, W.H.; Rush, J.D. Reduction potential of the carbon dioxide/carbon dioxide radical anion: A comparison with other C1 radicals. *J. Phys. Chem.* **1987**, *91*, 4429–4430. [CrossRef]
13. Wardman, P. Reduction Potentials of One-Electron Couples Involving Free Radicals in Aqueous Solution. *J. Phys. Chem. Ref. Data* **1989**, *18*, 1637–1755. [CrossRef]
14. Subramanian, V.; Wolf, E.E.; Kamat, P.V. Green Emission to Probe Photoinduced Charging Events in ZnO−Au Nanoparticles. Charge Distribution and Fermi-Level Equilibration. *J. Phys. Chem. B* **2003**, *107*, 7479–7485. [CrossRef]
15. Puga, A.V. Photocatalytic production of hydrogen from biomass-derived feedstocks. *Coord. Chem. Rev.* **2016**, *315*, 1–66. [CrossRef]
16. Fujishima, A.; Honda, K. Electrochemical Photolysis of Water at a Semiconductor Electrode. *Nature* **1972**, *238*, 37–38. [CrossRef] [PubMed]

17. Coehn, A. Studien über photochemische Gleichgewichte. IV. Das Lichtgleichgewicht Knallgas-Wasserdampf. *Berichte der Deutschen Chemischen Gesellschaft* **1910**, *43*, 880–884. [CrossRef]
18. Fujishima, A.; Honda, K.I.; Kikuchi, S.I. Photosensitized Electrolytic Oxidation on Semiconducting n-Type $TiO_2$ Electrode. *J. Soc. Chem. Ind. Jpn.* **1969**, *72*, 108–113. [CrossRef]
19. Fujishima, A.; Honda, K. Evidence of Photosensitized Electrolytic Oxidation on $TiO_2$ Electrode from pH Change of Electrolyte Solution. *J. Soc. Chem. Ind. Jpn.* **1971**, *74*, 355–358. [CrossRef]
20. Fujishima, A.; Sugiyama, E.; Honda, K. Photosensitized Electrolytic Oxidation of Iodide Ions on Cadmium Sulfide Single Crystal Electrode. *Bull. Chem. Soc. Jpn.* **1971**, *44*, 304. [CrossRef]
21. Fujishima, A.; Honda, K.J. *Seisan Kenkyu*; Institute of Industrial Science, University of Tokyo: Tokyo, Japan, 1970; Volume 22, p. 478.
22. Available online: https://www.scopus.com/record/pubmetrics.uri?eid=2-s2.0-35348875044&origin=recordpage (accessed on 25 October 2018).
23. Fenner, F.; Henderson, D.A.; Arita, I.; Jezek, Z.; Ladnyi, I.D. *Smallpox and Its Eradication*; World Health Organization: Geneva, Switzerland, 1988.
24. Frank, S.N.; Bard, A.J. Semiconductor electrodes. 12. Photoassisted oxidations and photoelectrosynthesis at polycrystalline titanium dioxide electrodes. *J. Am. Chem. Soc.* **1977**, *99*, 4667–4675. [CrossRef]
25. Tooru, I.; Tadashi, W.; Akira, F.; Kenichi, H. Competitive photosensitized oxidation at tio2 photoanode. *Chem. Lett.* **1977**, *6*, 1073–1076. [CrossRef]
26. Kraeutler, B.; Bard, A.J. Photoelectrosynthesis of ethane from acetate ion at an n-type titanium dioxide electrode. The photo-Kolbe reaction. *J. Am. Chem. Soc.* **1977**, *99*, 7729–7731. [CrossRef]
27. Dutoit, E.C.; Cardon, F.; Gomes, W.P. Electrochemical Properties of the Semiconducting $TiO_2$ (Rutile) Single Crystal Electrode. *Berichte Bunsenges. Phys. Chem.* **1976**, *80*, 475–481. [CrossRef]
28. Kalyanasundaram, K.; Grätzel, M. Cyclic Cleavage of Water into $H_2$ and $O_2$ by Visible Light with Coupled Redox Catalysts. *Angew. Chem. Int. Ed. Engl.* **1979**, *18*, 701–702. [CrossRef]
29. Borgarello, E.; Kiwi, J.; Pelizzetti, E.; Visca, M.; Grätzel, M. Photochemical cleavage of water by photocatalysis. *Nature* **1981**, *289*, 158. [CrossRef]
30. Graetzel, M. Artificial photosynthesis: Water cleavage into hydrogen and oxygen by visible light. *Accounts Chem. Res.* **1981**, *14*, 376–384. [CrossRef]
31. Schrauzer, G.N.; Guth, T.D. Photocatalytic reactions. 1. Photolysis of water and photoreduction of nitrogen on titanium dioxide. *J. Am. Chem. Soc.* **1977**, *99*, 7189–7193. [CrossRef]
32. Bard, A.J. Photoelectrochemistry and heterogeneous photo-catalysis at semiconductors. *J. Photochem.* **1979**, *10*, 59–75. [CrossRef]
33. Green, M.A.; Emery, K.; Hishikawa, Y.; Warta, W.; Dunlop, E.D. Solar cell efficiency tables (Version 45). *Prog. Photovolt. Res. Appl.* **2014**, *23*, 1–9. [CrossRef]
34. Frank, S.N.; Bard, A.J. Heterogeneous photocatalytic oxidation of cyanide ion in aqueous solutions at titanium dioxide powder. *J. Am. Chem. Soc.* **1977**, *99*, 303–304. [CrossRef]
35. Minero, C.; Lorenzi, E.; Pramauro, E.; Pelizzetti, E. Dioxygen evolution from inorganic systems. Water oxidation mediated by $RuO_2$ and $TiO_2$-$RuO_2$ Colloids. *Inorganica Chim. Acta* **1984**, *91*, 301–305. [CrossRef]
36. Yamakata, A.; Ishibashi, T.-a.; Onishi, H. Electron- and Hole-Capture Reactions on Pt/$TiO_2$ Photocatalyst Exposed to Methanol Vapor Studied with Time-Resolved Infrared Absorption Spectroscopy. *J. Phys. Chem. B* **2002**, *106*, 9122–9125. [CrossRef]
37. Yamakata, A.; Ishibashi, T.-A.; Onishi, H. Effects of accumulated electrons on the decay kinetics of photogenerated electrons in Pt/$TiO_2$ photocatalyst studied by time-resolved infrared absorption spectroscopy. *J. Photochem. Photobiol. A Chem.* **2003**, *160*, 33–36. [CrossRef]
38. Baba, R.; Nakabayashi, S.; Fujishima, A.; Honda, K. Investigation of the mechanism of hydrogen evolution during photocatalytic water decomposition on metal-loaded semiconductor powders. *J. Phys. Chem.* **1985**, *89*, 1902–1905. [CrossRef]
39. Yamakata, A.; Ishibashi, T.-a.; Onishi, H. Effects of Water Addition on the Methanol Oxidation on Pt/$TiO_2$ Photocatalyst Studied by Time-Resolved Infrared Absorption Spectroscopy. *J. Phys. Chem. B* **2003**, *107*, 9820–9823. [CrossRef]
40. Panayotov, D.A.; Morris, J.R. Surface chemistry of Au/$TiO_2$: Thermally and photolytically activated reactions. *Surf. Sci. Rep.* **2016**, *71*, 77–271. [CrossRef]

41. Yang, X.; Tamai, N. How fast is interfacial hole transfer? In situ monitoring of carrier dynamics in anatase $TiO_2$ nanoparticles by femtosecond laser spectroscopy. *Phys. Chem. Chem. Phys.* **2001**, *3*, 3393–3398. [CrossRef]
42. Chen, T.; Feng, Z.; Wu, G.; Shi, J.; Ma, G.; Ying, P.; Li, C. Mechanistic Studies of Photocatalytic Reaction of Methanol for Hydrogen Production on $Pt/TiO_2$ by in situ Fourier Transform IR and Time-Resolved IR Spectroscopy. *J. Phys. Chem. C* **2007**, *111*, 8005–8014. [CrossRef]
43. Iwata, K.; Takaya, T.; Hamaguchi, H.-O.; Yamakata, A.; Ishibashi, T.-A.; Onishi, H.; Kuroda, H. Carrier Dynamics in $TiO_2$ and $Pt/TiO_2$ Powders Observed by Femtosecond Time-Resolved Near-Infrared Spectroscopy at a Spectral Region of 0.9−1.5 μm with the Direct Absorption Method. *J. Phys. Chem. B* **2004**, *108*, 20233–20239. [CrossRef]
44. Fang, Y.-H.; Wei, G.-F.; Liu, Z.-P. Catalytic Role of Minority Species and Minority Sites for Electrochemical Hydrogen Evolution on Metals: Surface Charging, Coverage, and Tafel Kinetics. *J. Phys. Chem. C* **2013**, *117*, 7669–7680. [CrossRef]
45. Chiarello, G.L.; Aguirre, M.H.; Selli, E. Hydrogen production by photocatalytic steam reforming of methanol on noble metal-modified $TiO_2$. *J. Catal.* **2010**, *273*, 182–190. [CrossRef]
46. Zeradjanin, A.R.; Grote, J.-P.; Polymeros, G.; Mayrhofer, K.J.J. A Critical Review on Hydrogen Evolution Electrocatalysis: Re-exploring the Volcano-relationship. *Electroanalysis* **2016**, *28*, 2256–2269. [CrossRef]
47. Santos, E.; Quaino, P.; Schmickler, W. Theory of electrocatalysis: Hydrogen evolution and more. *Phys. Chem. Chem. Phys.* **2012**, *14*, 11224–11233. [CrossRef]
48. Calza, P.; Minella, M.; Demarchis, L.; Sordello, F.; Minero, C. Photocatalytic rate dependence on light absorption properties of different $TiO_2$ specimens. *Catal. Today* **2018**. [CrossRef]
49. Gordon, T.R.; Cargnello, M.; Paik, T.; Mangolini, F.; Weber, R.T.; Fornasiero, P.; Murray, C.B. Nonaqueous Synthesis of $TiO_2$ Nanocrystals Using $TiF_4$ to Engineer Morphology, Oxygen Vacancy Concentration, and Photocatalytic Activity. *J. Am. Chem. Soc.* **2012**, *134*, 6751–6761. [CrossRef] [PubMed]
50. Habas, S.E.; Lee, H.; Radmilovic, V.; Somorjai, G.A.; Yang, P. Shaping binary metal nanocrystals through epitaxial seeded growth. *Nat. Mater.* **2007**, *6*, 692–697. [CrossRef]
51. Buonsanti, R.; Grillo, V.; Carlino, E.; Giannini, C.; Kipp, T.; Cingolani, R.; Cozzoli, P.D. Nonhydrolytic synthesis of high-quality anisotropically shaped brookite $TiO_2$ nanocrystals. *J. Am. Chem. Soc.* **2008**, *130*, 11223–11233. [CrossRef] [PubMed]
52. Tsung, C.K.; Kuhn, J.N.; Huang, W.; Aliaga, C.; Hung, L.I.; Somorjai, G.A.; Yang, P. Sub-10 nm platinum nanocrystals with size and shape control: Catalytic study for ethylene and pyrrole hydrogenation. *J. Am. Chem. Soc.* **2009**, *131*, 5816–5822. [CrossRef] [PubMed]
53. Tao, A.; Sinsermsuksakul, P.; Yang, P. Polyhedral silver nanocrystals with distinct scattering signatures. *Angew. Chem. Int. Ed. Engl.* **2006**, *45*, 4597–4601. [CrossRef]
54. Hochbaum, A.I.; Yang, P. Semiconductor nanowires for energy conversion. *Chem. Rev.* **2010**, *110*, 527–546. [CrossRef]
55. Xia, Y.; Xiong, Y.; Lim, B.; Skrabalak, S.E. Shape-controlled synthesis of metal nanocrystals: Simple chemistry meets complex physics? *Angew. Chem. Int. Ed. Engl.* **2009**, *48*, 60–103. [CrossRef]
56. Lim, B.; Kobayashi, H.; Yu, T.; Wang, J.; Kim, M.J.; Li, Z.Y.; Rycenga, M.; Xia, Y. Synthesis of Pd-Au bimetallic nanocrystals via controlled overgrowth. *J. Am. Chem. Soc.* **2010**, *132*, 2506–2507. [CrossRef]
57. Yin, Y.; Erdonmez, C.; Aloni, S.; Alivisatos, A.P. Faceting of nanocrystals during chemical transformation: From solid silver spheres to hollow gold octahedra. *J. Am. Chem. Soc.* **2006**, *128*, 12671–12673. [CrossRef]
58. Feng, X.; Zhai, J.; Jiang, L. The fabrication and switchable superhydrophobicity of $TiO_2$ nanorod films. *Angew. Chem. Int. Ed. Engl.* **2005**, *44*, 5115–5118. [CrossRef] [PubMed]
59. Yi, Z.; Ye, J.; Kikugawa, N.; Kako, T.; Ouyang, S.; Stuart-Williams, H.; Yang, H.; Cao, J.; Luo, W.; Li, Z.; et al. An orthophosphate semiconductor with photooxidation properties under visible-light irradiation. *Nat. Mater.* **2010**, *9*, 559–564. [CrossRef] [PubMed]
60. Diebold, U. The surface science of titanium dioxide. *Surf. Sci. Rep.* **2003**, *48*, 53–229. [CrossRef]
61. Gong, X.Q.; Selloni, A.; Batzill, M.; Diebold, U. Steps on anatase $TiO_2$(101). *Nat Mater* **2006**, *5*, 665–670. [CrossRef] [PubMed]
62. Setvin, M.; Hulva, J.; Wang, H.H.; Simschitz, T.; Schmid, M.; Parkinson, G.S.; Di Valentin, C.; Selloni, A.; Diebold, U. Formaldehyde Adsorption on the Anatase $TiO_2$(101) Surface: Experimental and Theoretical Investigation. *J. Phys. Chem. C* **2017**, *121*, 8914–8922. [CrossRef]

63. Selcuk, S.; Selloni, A. Facet-dependent trapping and dynamics of excess electrons at anatase $TiO_2$ surfaces and aqueous interfaces. *Nat. Mater.* **2016**, *15*, 1107. [CrossRef] [PubMed]
64. Setvin, M.; Aschauer, U.; Hulva, J.; Simschitz, T.; Daniel, B.; Schmid, M.; Selloni, A.; Diebold, U. Following the Reduction of Oxygen on $TiO_2$ Anatase (101) Step by Step. *J. Am. Chem. Soc.* **2016**, *138*, 9565–9571. [CrossRef] [PubMed]
65. Setvin, M.; Buchholz, M.; Hou, W.Y.; Zhang, C.; Stoger, B.; Hulva, J.; Simschitz, T.; Shi, X.; Pavelec, J.; Parkinson, G.S.; et al. A Multitechnique Study of CO Adsorption on the $TiO_2$ Anatase (101) Surface. *J. Phys. Chem. C* **2015**, *119*, 21044–21052. [CrossRef]
66. Dulub, O.; Batzilln, M.; Solovev, S.; Loginova, E.; Alchagirov, A.; Madey, T.E.; Diebold, U. Electron-induced oxygen desorption from the $TiO_2$(011)-2x1 surface leads to self-organized vacancies. *Science* **2007**, *317*, 1052–1056. [CrossRef] [PubMed]
67. Li, S.-C.; Chu, L.-N.; Gong, X.-Q.; Diebold, U. Hydrogen bonding controls the dynamics of catechol adsorbed on a $TiO_2$(110) surface. *J. Mater. Chem.* **2010**, *20*, 10319. [CrossRef]
68. Kavan, L.; Gratzel, M.; Gilbert, S.E.; Klemenz, C.; Scheel, H.J. Electrochemical and photoelectrochemical investigation of single-crystal anatase. *J. Am. Chem. Soc.* **1996**, *118*, 6716–6723. [CrossRef]
69. Jang, E.S.; Won, J.H.; Hwang, S.J.; Choy, J.H. Fine Tuning of the Face Orientation of ZnO Crystals to Optimize Their Photocatalytic Activity. *Adv. Mater.* **2006**, *18*, 3309–3312. [CrossRef]
70. Mino, L.; Pellegrino, F.; Rades, S.; Radnik, J.; Hodoroaba, V.-D.; Spoto, G.; Maurino, V.; Martra, G. Beyond Shape Engineering of $TiO_2$ Nanoparticles: Post-Synthesis Treatment Dependence of Surface Hydration, Hydroxylation, Lewis Acidity and Photocatalytic Activity of $TiO_2$ Anatase Nanoparticles with Dominant {001} or {101} Facets. *ACS Appl. Nano Mater.* **2018**. [CrossRef]
71. Gong, X.Q.; Selloni, A. Reactivity of anatase $TiO_2$ nanoparticles: The role of the minority (001) surface. *J. Phys. Chem. B* **2005**, *109*, 19560–19562. [CrossRef] [PubMed]
72. Vittadini, A.; Selloni, A.; Rotzinger, F.P.; Gratzel, M. Structure and energetics of water adsorbed at $TiO_2$ anatase (101) and (001) surfaces. *Phys. Rev. Lett.* **1998**, *81*, 2954–2957. [CrossRef]
73. Selloni, A. Crystal growth—Anatase shows its reactive side. *Nat. Mater.* **2008**, *7*, 613–615. [CrossRef] [PubMed]
74. Vittadini, A.; Casarin, M.; Selloni, A. Chemistry of and on $TiO_2$-anatase surfaces by DFT calculations: A partial review. *Theor. Chem. Accounts* **2007**, *117*, 663–671. [CrossRef]
75. Pan, J.; Liu, G.; Lu, G.Q.; Cheng, H.M. On the true photoreactivity order of {001}, {010}, and {101} facets of anatase $TiO_2$ crystals. *Angew. Chem. Int. Ed. Engl.* **2011**, *50*, 2133–2137. [CrossRef] [PubMed]
76. Wulff, G. Zur Frage der Geschwindigkeit des Wachstums und der Auflösung der Krystallflächen. *Z. Kryst. Miner.* **1901**, 449–530.
77. Ramamoorthy, M.; Vanderbilt, D.; King-Smith, R.D. First-principles calculations of the energetics of stoichiometric $TiO_2$ surfaces. *Phys. Rev. B Condens Matter* **1994**, *49*, 16721–16727. [CrossRef]
78. Gong, X.-Q.; Selloni, A. First-principles study of the structures and energetics of stoichiometric brookite $TiO_2$ surfaces. *Phys. Rev. B* **2007**, *76*. [CrossRef]
79. Barnard, A.S.; Zapol, P.; Curtiss, L.A. Modeling the Morphology and Phase Stability of $TiO_2$ Nanocrystals in Water. *J. Chem. Theo. Comput.* **2005**, *1*, 107–116. [CrossRef] [PubMed]
80. Van de Hulst, H.C. Light scattering by small particles. *Q. J. R. Meteorol. Soc.* **1958**, *84*, 198–199. [CrossRef]
81. Mackowski, D.W.; Mishchenko, M.I. Calculation of the T matrix and the scattering matrix for ensembles of spheres. *J. Opt. Soc. of Am. Opt. Image Sci. Vis.* **1996**, *13*, 2266–2278. [CrossRef]
82. Yun, H.J.; Lee, H.; Jool, J.B.; Kim, N.D.; Yi, J. Effect of $TiO_2$ nanoparticle shape on hydrogen evolution via water splitting. *J. Nanosci. Nanotechnol.* **2011**, *11*, 1688–1691. [CrossRef] [PubMed]
83. Cho, I.S.; Chen, Z.B.; Forman, A.J.; Kim, D.R.; Rao, P.M.; Jaramillo, T.F.; Zheng, X.L. Branched $TiO_2$ Nanorods for Photoelectrochemical Hydrogen Production. *Nano Lett.* **2011**, *11*, 4978–4984. [CrossRef] [PubMed]
84. Jiang, Z.; Tang, Y.; Tay, Q.; Zhang, Y.; Malyi, O.I.; Wang, D.; Deng, J.; Lai, Y.; Zhou, H.; Chen, X.; et al. Understanding the Role of Nanostructures for Efficient Hydrogen Generation on Immobilized Photocatalysts. *Adv. Energy Mater.* **2013**, *3*, 1368–1380. [CrossRef]
85. Joannopoulos, J.D.; Johnson, S.G.; Winn, J.N.; Meade, R.D. *Photonic Crystals Molding the Flow of Light*, 2nd ed.; Princeton University Press: Princeton, NJ, USA, 2008.
86. Baba, T. Slow light in photonic crystals. *Nat. Photonics* **2008**, *2*, 465–473. [CrossRef]

87. Zhao, Y.; Zhao, H.-W.; Zhang, X.-Y.; Yuan, B.; Zhang, S. New mechanisms of slow light and their applications. *Opt. Laser Technol.* **2009**, *41*, 517–525. [CrossRef]
88. Sordello, F.; Minero, C. Photocatalytic hydrogen production on Pt-loaded $TiO_2$ inverse opals. *Appl. Catal. B Environ.* **2015**, *163*, 452–458. [CrossRef]
89. Chen, J.I.L.; von Freymann, G.; Choi, S.Y.; Kitaev, V.; Ozin, G.A. Slow photons in the fast lane in chemistry. *J. Mater. Chem.* **2008**, *18*, 369–373. [CrossRef]
90. Sordello, F.; Duca, C.; Maurino, V.; Minero, C. Photocatalytic metamaterials: $TiO_2$ inverse opals. *Chem. Commun.* **2011**, *47*, 6147–6149. [CrossRef] [PubMed]
91. Chiarello, G.L.; Zuliani, A.; Ceresoli, D.; Martinazzo, R.; Selli, E. Exploiting the Photonic Crystal Properties of $TiO_2$ Nanotube Arrays To Enhance Photocatalytic Hydrogen Production. *ACS Catal.* **2016**, *6*, 1345–1353. [CrossRef]
92. D'Arienzo, M.; Dozzi, M.V.; Redaelli, M.; Di Credico, B.; Morazzoni, F.; Scotti, R.; Polizzi, S. Crystal Surfaces and Fate of Photogenerated Defects in Shape-Controlled Anatase Nanocrystals: Drawing Useful Relations to Improve the $H_2$ Yield in Methanol Photosteam Reforming. *J. Phys. Chem. C* **2015**, *119*, 12385–12393. [CrossRef]
93. Meng, A.; Zhang, J.; Xu, D.; Cheng, B.; Yu, J. Enhanced photocatalytic $H_2$-production activity of anatase $TiO_2$ nanosheet by selectively depositing dual-cocatalysts on {101} and {001} facets. *Appl. Catal. B Environ.* **2016**, *198*, 286–294. [CrossRef]
94. Yu, J.; Low, J.; Xiao, W.; Zhou, P.; Jaroniec, M. Enhanced photocatalytic $CO_2$-reduction activity of anatase $TiO_2$ by coexposed {001} and {101} facets. *J. Am. Chem. Soc.* **2014**, *136*, 8839–8842. [CrossRef] [PubMed]
95. Liu, J.; Olds, D.; Peng, R.; Yu, L.; Foo, G.S.; Qian, S.; Keum, J.; Guiton, B.S.; Wu, Z.L.; Page, K. Quantitative Analysis of the Morphology of {101} and {001} Faceted Anatase $TiO_2$ Nanocrystals and Its Implication on Photocatalytic Activity. *Chem. Mater.* **2017**, *29*, 5591–5604. [CrossRef]
96. Chiarello, G.L.; Dozzi, M.V.; Scavini, M.; Grunwaldt, J.D.; Selli, E. One step flame-made fluorinated Pt/$TiO_2$ photocatalysts for hydrogen production. *Appl. Catal. B Environ.* **2014**, *160–161*, 144–151. [CrossRef]
97. Yu, J.; Qi, L.; Jaroniec, M. Hydrogen Production by Photocatalytic Water Splitting over Pt/$TiO_2$ Nanosheets with Exposed (001) Facets. *J. Phys. Chem. C* **2010**, *114*, 13118–13125. [CrossRef]
98. Amano, F.; Prieto-Mahaney, O.-O.; Terada, Y.; Yasumoto, T.; Shibayama, T.; Ohtani, B. Decahedral Single-Crystalline Particles of Anatase Titanium(IV) Oxide with High Photocatalytic Activity. *Chem. Mater.* **2009**, *21*, 2601–2603. [CrossRef]
99. Chiarello, G.L.; Selli, E.; Forni, L. Photocatalytic hydrogen production over flame spray pyrolysis-synthesised $TiO_2$ and Au/$TiO_2$. *Appl. Catal. B Environ.* **2008**, *84*, 332–339. [CrossRef]
100. Naldoni, A.; D'Arienzo, M.; Altomare, M.; Marelli, M.; Scotti, R.; Morazzoni, F.; Selli, E.; Dal Santo, V. Pt and Au/$TiO_2$ photocatalysts for methanol reforming: Role of metal nanoparticles in tuning charge trapping properties and photoefficiency. *Appl. Catal. B Environ.* **2013**, *130–131*, 239–248. [CrossRef]
101. Jones, W.; Martin, D.J.; Caravaca, A.; Beale, A.M.; Bowker, M.; Maschmeyer, T.; Hartley, G.; Masters, A. A comparison of photocatalytic reforming reactions of methanol and triethanolamine with Pd supported on titania and graphitic carbon nitride. *Appl. Catal. B Environ.* **2017**, *240*, 373–379. [CrossRef]
102. Daskalaki, V.M.; Kondarides, D.I. Efficient production of hydrogen by photo-induced reforming of glycerol at ambient conditions. *Catal. Today* **2009**, *144*, 75–80. [CrossRef]
103. López-Tenllado, F.J.; Hidalgo-Carrillo, J.; Montes, V.; Marinas, A.; Urbano, F.J.; Marinas, J.M.; Ilieva, L.; Tabakova, T.; Reid, F. A comparative study of hydrogen photocatalytic production from glycerol and propan-2-ol on M/$TiO_2$ systems (M = Au, Pt, Pd). *Catal. Today* **2017**, *280*, 58–64. [CrossRef]
104. Melchionna, M.; Beltram, A.; Montini, T.; Monai, M.; Nasi, L.; Fornasiero, P.; Prato, M. Highly efficient hydrogen production through ethanol photoreforming by a carbon nanocone/Pd@$TiO_2$ hybrid catalyst. *Chem. Commun.* **2016**, *52*, 764–767. [CrossRef] [PubMed]
105. Velázquez, J.J.; Fernández-González, R.; Díaz, L.; Pulido Melián, E.; Rodríguez, V.D.; Núñez, P. Effect of reaction temperature and sacrificial agent on the photocatalytic $H_2$-production of Pt-$TiO_2$. *J. Alloys Compd.* **2017**, *721*, 405–410. [CrossRef]
106. López, C.R.; Melián, E.P.; Ortega Méndez, J.A.; Santiago, D.E.; Doña Rodríguez, J.M.; González Díaz, O. Comparative study of alcohols as sacrificial agents in $H_2$ production by heterogeneous photocatalysis using Pt/$TiO_2$ catalysts. *J. Photochem. Photobiol. A Chem.* **2015**, *312*, 45–54. [CrossRef]

107. Kennedy, J.; Bahruji, H.; Bowker, M.; Davies, P.R.; Bouleghlimat, E.; Issarapanacheewin, S. Hydrogen generation by photocatalytic reforming of potential biofuels: Polyols, cyclic alcohols, and saccharides. *J. Photochem. Photobiol. A Chem.* **2018**, *356*, 451–456. [CrossRef]
108. Bahruji, H.; Bowker, M.; Davies, P.R.; Pedrono, F. New insights into the mechanism of photocatalytic reforming on Pd/$TiO_2$. *Appl. Catal. B Environ.* **2011**, *107*, 205–209. [CrossRef]
109. Taylor, S.; Mehta, M.; Samokhvalov, A. Production of hydrogen by glycerol photoreforming using binary nitrogen-metal-promoted N-M-$TiO_2$ photocatalysts. *Chemphyschem* **2014**, *15*, 942–949. [CrossRef]
110. Zhang, L.; Wang, W.; Zeng, S.; Su, Y.; Hao, H. Enhanced $H_2$ evolution from photocatalytic cellulose conversion based on graphitic carbon layers on $TiO_2$/$NiO_x$. *Green Chem.* **2018**, *20*, 3008–3013. [CrossRef]
111. Wang, C.; Cai, X.; Chen, Y.; Cheng, Z.; Luo, X.; Mo, S.; Jia, L.; Shu, R.; Lin, P.; Yang, Z.; et al. Efficient hydrogen production from glycerol photoreforming over $Ag_2O$ $TiO_2$ synthesized by a sol–gel method. *Int. J. Hydrogen Energy* **2017**, *42*, 17063–17074. [CrossRef]
112. Berto, T.F.; Sanwald, K.E.; Eisenreich, W.; Gutiérrez, O.Y.; Lercher, J.A. Photoreforming of ethylene glycol over Rh/$TiO_2$ and Rh/GaN:ZnO. *J. Catal.* **2016**, *338*, 68–81. [CrossRef]
113. Sanwald, K.E.; Berto, T.F.; Eisenreich, W.; Gutiérrez, O.Y.; Lercher, J.A. Catalytic routes and oxidation mechanisms in photoreforming of polyols. *J. Catal.* **2016**, *344*, 806–816. [CrossRef]
114. Caravaca, A.; Jones, W.; Hardacre, C.; Bowker, M. $H_2$ production by the photocatalytic reforming of cellulose and raw biomass using Ni, Pd, Pt and Au on titania. *Proc. Math. Phys. Eng. Sci.* **2016**, *472*, 20160054. [CrossRef] [PubMed]
115. Kawai, T.; Sakata, T. Photocatalytic decomposition of gaseous water over $TiO_2$ and $TiO_2$—$RuO_2$ surfaces. *Chem. Phys. Lett.* **1980**, *72*, 87–89. [CrossRef]
116. Nie, Y.-C.; Yu, F.; Wang, L.-C.; Xing, Q.-J.; Liu, X.; Pei, Y.; Zou, J.-P.; Dai, W.-L.; Li, Y.; Suib, S.L. Photocatalytic degradation of organic pollutants coupled with simultaneous photocatalytic $H_2$ evolution over graphene quantum dots/Mn-N-$TiO_2$ /g-$C_3N_4$ composite catalysts: Performance and mechanism. *Appl. Catal. B Environ.* **2018**, *227*, 312–321. [CrossRef]
117. Yu, X.; Fan, X.; An, L.; Liu, G.; Li, Z.; Liu, J.; Hu, P. Mesocrystalline $Ti^{3+}TiO_2$ hybridized g-$C_3N_4$ for efficient visible-light photocatalysis. *Carbon* **2018**, *128*, 21–30. [CrossRef]
118. Wu, M.; Zhang, J.; Liu, C.; Gong, Y.; Wang, R.; He, B.; Wang, H. Rational Design and Fabrication of Noble-metal-free NixP Cocatalyst Embedded 3D N-$TiO_2$/g-$C_3N_4$ Heterojunctions with Enhanced Photocatalytic Hydrogen Evolution. *ChemCatChem* **2018**, *10*, 3069–3077. [CrossRef]
119. Yang, C.; Qin, J.; Xue, Z.; Ma, M.; Zhang, X.; Liu, R. Rational design of carbon-doped $TiO_2$ modified g-$C_3N_4$ via in-situ heat treatment for drastically improved photocatalytic hydrogen with excellent photostability. *Nano Energy* **2017**, *41*, 1–9. [CrossRef]
120. Xiang, Q.; Yu, J.; Jaroniec, M. Enhanced photocatalytic $H_2$-production activity of graphene-modified titania nanosheets. *Nanoscale* **2011**, *3*, 3670–3678. [CrossRef]
121. Chai, B.; Peng, T.; Mao, J.; Li, K.; Zan, L. Graphitic carbon nitride (g-C3N4)-Pt-$TiO_2$ nanocomposite as an efficient photocatalyst for hydrogen production under visible light irradiation. *Phys. Chem. Chem. Phys.* **2012**, *14*, 16745–16752. [CrossRef] [PubMed]
122. Giovannetti, R.; Rommozzi, E.; Zannotti, M.; D'Amato, C.A. Recent Advances in Graphene Based $TiO_2$ Nanocomposites (GTiO2Ns) for Photocatalytic Degradation of Synthetic Dyes. *Catalysts* **2017**, *7*, 305. [CrossRef]
123. Minella, M.; Sordello, F.; Minero, C. Photocatalytic process in $TiO_2$/graphene hybrid materials. Evidence of charge separation by electron transfer from reduced graphene oxide to $TiO_2$. *Catal. Today* **2017**, *281*, 29–37. [CrossRef]
124. Pastrana-Martínez, L.M.; Morales-Torres, S.; Likodimos, V.; Figueiredo, J.L.; Faria, J.L.; Falaras, P.; Silva, A.M.T. Advanced nanostructured photocatalysts based on reduced graphene oxide–$TiO_2$ composites for degradation of diphenhydramine pharmaceutical and methyl orange dye. *Appl. Catal. B Environ.* **2012**, *123–124*, 241–256. [CrossRef]
125. Qianqian, Z.; Tang, B.; Guoxin, H. High photoactive and visible-light responsive graphene/titanate nanotubes photocatalysts: Preparation and characterization. *J. Hazard. Mater.* **2011**, *198*, 78–86. [CrossRef]
126. Long, R.; English, N.J.; Prezhdo, O.V. Photo-induced Charge Separation across the Graphene–$TiO_2$ Interface Is Faster than Energy Losses: A Time-Domain ab Initio Analysis. *J. Am. Chem. Soc.* **2012**, *134*, 14238–14248. [CrossRef]

127. Wang, Y.; Shi, R.; Lin, J.; Zhu, Y. Significant photocatalytic enhancement in methylene blue degradation of $TiO_2$ photocatalysts via graphene-like carbon in situ hybridization. *Appl. Catal. B Environ.* **2010**, *100*, 179–183. [CrossRef]
128. Minella, M.; Fabbri, D.; Calza, P.; Minero, C. Selected hybrid photocatalytic materials for the removal of drugs from water. *Curr. Opin. Green Sustain. Chem.* **2017**, *6*, 11–17. [CrossRef]
129. Tang, B.; Chen, H.; Peng, H.; Wang, Z.; Huang, W. Graphene Modified $TiO_2$ Composite Photocatalysts: Mechanism, Progress and Perspective. *Nano Mater.* **2018**, *8*, 105. [CrossRef] [PubMed]
130. Lucchetti, R.; Siciliano, A.; Clarizia, L.; Russo, D.; Di Somma, I.; Di Natale, F.; Guida, M.; Andreozzi, R.; Marotta, R. Sacrificial photocatalysis: Removal of nitrate and hydrogen production by nano-copper-loaded P25 titania. A kinetic and ecotoxicological assessment. *Environ. Sci. Pollut. Res. Int.* **2017**, *24*, 5898–5907. [CrossRef]
131. Chen, W.; Wang, Y.; Liu, S.; Gao, L.; Mao, L.; Fan, Z.; Shangguan, W.; Jiang, Z. Non-noble metal Cu as a cocatalyst on $TiO_2$ nanorod for highly efficient photocatalytic hydrogen production. *Appl. Surf. Sci.* **2018**, *445*, 527–534. [CrossRef]
132. Segovia-Guzmán, M.O.; Román-Aguirre, M.; Verde-Gomez, J.Y.; Collins-Martínez, V.H.; Zaragoza-Galán, G.; Ramos-Sánchez, V.H. Green $Cu_2O/TiO_2$ heterojunction for glycerol photoreforming. *Catal. Today* **2018**. [CrossRef]
133. Ampelli, C.; Passalacqua, R.; Genovese, C.; Perathoner, S.; Centi, G.; Montini, T.; Gombac, V.; Fornasiero, P. Solar Energy and Biowaste Conversion into $H_2$ on $CuO_x/TiO_2$ Nanocomposites. *Chem. Eng. Trans.* **2013**, *35*. [CrossRef]
134. Praveen Kumar, D.; Shankar, M.V.; Kumari, M.M.; Sadanandam, G.; Srinivas, B.; Durgakumari, V. Nano-size effects on $CuO/TiO_2$ catalysts for highly efficient $H_2$ production under solar light irradiation. *Chem. Commun.* **2013**, *49*, 9443–9445. [CrossRef] [PubMed]
135. Yu, J.; Ran, J. Facile preparation and enhanced photocatalytic $H_2$-production activity of $Cu(OH)_2$ cluster modified $TiO_2$. *Energy Environ. Sci.* **2011**, *4*, 1364. [CrossRef]
136. He, Z.; Fu, J.; Cheng, B.; Yu, J.; Cao, S. $Cu_2(OH)_2CO_3$ clusters: Novel noble-metal-free cocatalysts for efficient photocatalytic hydrogen production from water splitting. *Appl. Catal. B Environ.* **2017**, *205*, 104–111. [CrossRef]
137. Clarizia, L.; Spasiano, D.; Di Somma, I.; Marotta, R.; Andreozzi, R.; Dionysiou, D.D. Copper modified-$TiO_2$ catalysts for hydrogen generation through photoreforming of organics. A short review. *Int. J. Hydrogen Energy* **2014**, *39*, 16812–16831. [CrossRef]
138. Bonomo, M.; Dini, D.; Decker, F. Electrochemical and Photoelectrochemical Properties of Nickel Oxide (NiO) With Nanostructured Morphology for Photoconversion Applications. *Front. Chem.* **2018**, *6*. [CrossRef]
139. Kudo, A.; Miseki, Y. Heterogeneous photocatalyst materials for water splitting. *Chem. Soc. Rev.* **2009**, *38*, 253–278. [CrossRef] [PubMed]
140. Zhao, G.; Rui, K.; Dou, S.X.; Sun, W. Heterostructures for Electrochemical Hydrogen Evolution Reaction: A Review. *Adv. Funct. Mater.* **2018**, *28*, 1803291. [CrossRef]
141. Ott, J.; Gronemann, V.; Pontzen, F.; Fiedler, E.; Grossmann, G.; Kersebohm, D.B.; Weiss, G.; Witte, C. Methanol. *Ullmann's Encycl. Ind. Chem.* **2012**. [CrossRef]
142. Bowker, M.; Davies, P.R.; Al-Mazroai, L.S. Photocatalytic Reforming of Glycerol over Gold and Palladium as an Alternative Fuel Source. *Catal. Lett.* **2009**, *128*, 253–255. [CrossRef]
143. Matthews, R. Photocatalytic oxidation of chlorobenzene in aqueous suspensions of titanium dioxide. *J. Catal.* **1986**, *97*, 565–568. [CrossRef]
144. Hashimoto, K.; Kawai, T.; Sakata, T. Photocatalytic Reactions of Hydrocarbons and Fossil Fuels with Water. Hydrogen Production and Oxidation. *J. Phys. Chem.* **1984**, *88*, 4083–4088. [CrossRef]
145. Serpone, N.; Borgarello, E.; Harris, R.; Cahill, P.; Borgarello, M.; Pelizzetti, E. Photocatalysis over $TiO_2$ supported on a glass substrate. *Sol. Energy Mater.* **1986**, *14*, 121–127. [CrossRef]
146. Barbeni, M.; Pramauro, E.; Pelizzetti, E.; Borgarello, E.; Serpone, N.; Jamieson, M.A. Photochemical degradation of chlorinated dioxins, biphenyls phenols and benzene on semiconductor dispersion. *Chemosphere* **1986**, *15*, 1913–1916. [CrossRef]
147. Pelizzetti, E.; Borgarello, M.; Minero, C.; Pramauro, E.; Borgarello, E.; Serpone, N. Photocatalytic degradation of polychlorinated dioxins and polychlorinated biphenyls in aqueous suspensions of semiconductors irradiated with simulated solar light. *Chemosphere* **1988**, *17*, 499–510. [CrossRef]

148. Pelizzetti, E.; Minero, C. Mechanism of the photo-oxidative degradation of organic pollutants over $TiO_2$ particles. *Electrochim. Acta* **1993**, *38*, 47–55. [CrossRef]
149. Maurino, V.; Bedini, A.; Minella, M.; Rubertelli, F.; Pelizzetti, E.; Minero, C. Glycerol Transformation Through Photocatalysis: A Possible Route to Value Added Chemicals. *J. Adv. Oxid. Technol.* **2008**, *11*, 184–192. [CrossRef]
150. Minero, C.; Bedini, A.; Maurino, V. Glycerol as a probe molecule to uncover oxidation mechanism in photocatalysis. *Appl. Catal. B Environ.* **2012**, *128*, 135–143. [CrossRef]
151. Pellegrino, F.; Pellutiè, L.; Sordello, F.; Minero, C.; Ortel, E.; Hodoroaba, V.-D.; Maurino, V. Influence of agglomeration and aggregation on the photocatalytic activity of $TiO_2$ nanoparticles. *Appl. Catal. B Environ.* **2017**, *216*, 80–87. [CrossRef]
152. Binod, P.; Sindhu, R.; Singhania, R.R.; Vikram, S.; Devi, L.; Nagalakshmi, S.; Kurien, N.; Sukumaran, R.K.; Pandey, A. Bioethanol production from rice straw: An overview. *Bioresour. Technol.* **2010**, *101*, 4767–4774. [CrossRef] [PubMed]
153. Yang, Y.Z.; Chang, C.H.; Idriss, H. Photo-catalytic production of hydrogen form ethanol over $M/TiO_2$ catalysts (M = Pd, Pt or Rh). *Appl. Catal. B Environ.* **2006**, *67*, 217–222. [CrossRef]
154. Antoniadou, M.; Kondarides, D.I.; Lianos, P. Photooxidation Products of Ethanol During Photoelectrochemical Operation Using a Nanocrystalline Titania Anode and a Two Compartment Chemically Biased Cell. *Catal. Lett.* **2009**, *129*, 344–349. [CrossRef]
155. Kawai, T.; Sakata, T. Conversion of carbohydrate into hydrogen fuel by a photocatalytic process. *Nature* **1980**, *286*, 474–476. [CrossRef]
156. Sivasamy, A.; Cheah, K.Y.; Fornasiero, P.; Kemausuor, F.; Zinoviev, S.; Miertus, S. Catalytic applications in the production of biodiesel from vegetable oils. *ChemSusChem* **2009**, *2*, 278–300. [CrossRef]
157. Arechederra, R.L.; Treu, B.L.; Minteer, S.D. Development of glycerol/$O_2$ biofuel cell. *J. Power Sources* **2007**, *173*, 156–161. [CrossRef]
158. Zhang, Y.H.P. A sweet out-of-the-box solution to the hydrogen economy: Is the sugar-powered car science fiction? *Energy Environ. Sci.* **2009**, *2*, 272–282. [CrossRef]
159. Fu, X.; Long, J.; Wang, X.; Leung, D.Y.C.; Ding, Z.; Wu, L.; Zhang, Z.; Li, Z.; Fu, X. Photocatalytic reforming of biomass: A systematic study of hydrogen evolution from glucose solution. *Int. J. Hydrogen Energy* **2008**, *33*, 6484–6491. [CrossRef]
160. Cargnello, M.; Gasparotto, A.; Gombac, V.; Montini, T.; Barreca, D.; Fornasiero, P. Photocatalytic $H_2$ and Added-Value By-Products—The Role of Metal Oxide Systems in Their Synthesis from Oxygenates. *Eur. J. Inorg. Chem.* **2011**. [CrossRef]
161. Rossetti, I. Hydrogen Production by Photoreforming of Renewable Substrates. *ISRN Chem. Eng.* **2012**, *2012*, 1–21. [CrossRef]
162. Speltini, A.; Sturini, M.; Maraschi, F.; Dondi, D.; Serra, A.; Profumo, A.; Buttafava, A.; Albini, A. Swine sewage as sacrificial biomass for photocatalytic hydrogen gas production: Explorative study. *Int. J. Hydrogen Energy* **2014**, *39*, 11433–11440. [CrossRef]
163. Liu, C.; Lei, Z.; Yang, Y.; Zhang, Z. Preliminary trial on degradation of waste activated sludge and simultaneous hydrogen production in a newly-developed solar photocatalytic reactor with $AgX/TiO_2$-coated glass tubes. *Water Res.* **2013**, *47*, 4986–4992. [CrossRef] [PubMed]
164. Hans Wedepohl, K. The composition of the continental crust. *Geochim. Cosmochim. Acta* **1995**, *59*, 1217–1232. [CrossRef]
165. Hummers, W.S.; Offeman, R.E. Preparation of Graphitic Oxide. *J. Am. Chem. Soc.* **1958**, *80*, 1339. [CrossRef]
166. Huang, N.M.; Lim, H.N.; Chia, C.H.; Yarmo, M.A.; Muhamad, M.R. Simple room-temperature preparation of high-yield large-area graphene oxide. *Int. J. Nanomed.* **2011**, *6*, 3443–3448. [CrossRef]
167. Van Ruijven, B.; Lamarque, J.-F.; van Vuuren, D.P.; Kram, T.; Eerens, H. Emission scenarios for a global hydrogen economy and the consequences for global air pollution. *Glob. Environ. Chang.* **2011**, *21*, 983–994. [CrossRef]

168. Prather, M.J. Atmospheric science. An environmental experiment with $H_2$? *Science* **2003**, *302*, 581–582. [CrossRef]
169. Sanderson, M.G.; Collins, W.J.; Derwent, R.G.; Johnson, C.E. Simulation of global hydrogen levels using a lagrangian three-dimensional model. *J. Atmos. Chem.* **2003**, *46*, 15–28. [CrossRef]